An Arginine-Rich Motif in the ORF2 Capsid Protein Regulates the Hepatitis E Virus Lifecycle and Interactions with the Host Cell

Kévin Hervouet,[1,¶] Martin Ferrié,[1,¶] Maliki Ankavay,[1,¶,#] Claire Montpellier,[1] Charline Camuzet,[1] Virginie Alexandre,[1] Aïcha Dembélé,[1] Cécile Lecoeur,[1] Arnold Thomas Foe,[1] Peggy Bouquet,[2] David Hot,[2] Thibaut Vausselin,[1] Jean-Michel Saliou,[2] Sophie Salomé-Desnoulez,[2] Alexandre Vandeputte,[2] Laurent Marsollier,[3] Priscille Brodin,[1,2] Marlène Dreux,[4] Yves Rouillé,[1] Jean Dubuisson,[1] Cécile-Marie Aliouat-Denis,[1] Laurence Cocquerel,[1,*]

[1]University of Lille, CNRS, INSERM, CHU Lille, Pasteur Institute of Lille, U1019-UMR 9017-CIIL- Center for Infection and Immunity of Lille, Lille, France

[2]Univ. Lille, CNRS, Inserm, CHU Lille, Institut Pasteur de Lille, UMR2014 - US41 - PLBS-Plateformes Lilloises de Biologie & Santé, Lille, France.

[3]Equipe ATIP AVENIR, CRCINA, INSERM, University of Angers, Angers, France.

[4]CIRI - Centre International de Recherche en Infectiologie, Univ Lyon, Université Claude Bernard Lyon 1, Inserm-U1111, CNRS-UMR5308, ENS-Lyon, Lyon, France.

¶ These authors contributed equally to this work.

Present address: Division of Gastroenterology and Hepatology, Institute of Microbiology, Lausanne, Switzerland

* Corresponding author, laurence.cocquerel@cnrs.fr

Abstract

Hepatitis E virus (HEV) infection is the most common cause of acute viral hepatitis worldwide. Hepatitis E is usually asymptomatic and self-limiting but it can become chronic in immunocompromised patients and is associated with increased fulminant hepatic failure and mortality rates in pregnant women. HEV genome encodes three proteins including the ORF2 protein that is the viral capsid protein. Interestingly, HEV produces 3 isoforms of the ORF2 capsid protein which are partitioned in different subcellular compartments and perform distinct functions in the HEV lifecycle. Notably, the infectious ORF2 (ORF2i) protein is the structural component of virions, whereas the genome-free secreted and glycosylated ORF2 proteins likely act as a humoral immune decoy. Here, by using a series of ORF2 capsid protein mutants expressed in the infectious genotype 3 p6 HEV strain as well as chimeras between ORF2 and the CD4 glycoprotein, we demonstrated how an Arginine-Rich Motif (ARM) located in the ORF2 N-terminal region controls the fate and functions of ORF2 isoforms. We showed that the ARM controls ORF2 nuclear translocation, promoting regulation of host antiviral responses. This motif also regulates the dual topology and functionality of ORF2 signal peptide, leading to the production of either cytosolic infectious ORF2i or reticular non-infectious glycosylated ORF2 forms. It serves as maturation site of glycosylated ORF2 by cellular proteases, and promotes ORF2-host cell membrane interactions. The identification of ORF2 ARM as a unique central regulator of the HEV lifecycle uncovers how viruses settle strategies to condense their genetic information and hijack cellular processes.

48 # Author summary

49 Hepatitis E virus (HEV) is the major cause of acute viral hepatitis worldwide. Although
50 infection with HEV is usually self-resolving, it can cause up to 30% mortality in pregnant
51 women in the third trimester. There is no specific treatment nor universal vaccine to
52 fight against HEV. In our study, we focused on the HEV ORF2 capsid protein which is
53 produced as different forms that perform distinct functions in the HEV lifecycle. The
54 infectious ORF2i form is the structural component of virions, while the other forms likely
55 act as an immune decoy. Herein, we deciphered the molecular determinants of ORF2
56 multifunctionality. We identified an Arginine-Rich Motif (ARM) located in the ORF2 N-
57 terminal region that controls the subcellular localization, the fate and functions of ORF2
58 forms. It also promotes ORF2-host cell interactions. Our observations highlight the
59 ORF2 ARM as a unique central regulator of ORF2 addressing that finely controls the
60 HEV lifecycle.

61

62 # Introduction

63

64 Hepatitis E virus (HEV) is the most common cause of acute viral hepatitis worldwide
65 and is an emerging problem in industrialized countries. This virus causes about 20
66 million infections annually [1]. While HEV infection is asymptomatic for most patients,
67 some human populations including pregnant women and immunocompromised
68 patients have higher risk to develop severe forms and chronic infections, respectively.
69 HEV strains infecting humans have been classified into 4 main distinct genotypes (gt)
70 belonging to a single serotype [2]. Gt1 and gt2 that infect humans only, are primarily
71 transmitted through contaminated drinking water and are responsible for waterborne
72 hepatitis outbreaks in developing countries. In contrast, gt3 and gt4 are zoonotic and
73 are largely circulating in industrialized countries. They are mainly transmitted by
74 contact with swine and consumption of inadequately heated pork products [3]. There
75 is no specific treatment nor universal vaccine to fight against HEV.
76 HEV is a quasi-enveloped [4,5], positive-sense RNA virus expressing three open
77 reading frames (ORFs): ORF1, ORF2 and ORF3 [6]. ORF1 encodes the ORF1 non-
78 structural polyprotein that is the viral replicase [7]. ORF2 encodes the ORF2 viral
79 capsid protein and ORF3 encodes a small protein that is involved in virion
80 morphogenesis and egress [8,9] . Since studying the HEV lifecycle has long been
81 hampered by the absence of efficient systems to amplify HEV, many steps of the HEV
82 lifecycle remain poorly understood [10]. By combining the gt3 p6 strain [11] and a
83 highly transfectable subclone of PLC/PRF/5 cells (PLC3 cells), we previously
84 described an efficient HEV cell culture system [12]. This model notably enabled the
85 pioneering demonstration that, during its lifecycle, HEV produces at least 3 forms of
86 the ORF2 capsid protein: infectious ORF2 (ORF2i), glycosylated ORF2 (ORF2g), and

87 cleaved ORF2 (ORF2c). The ORF2i protein is the structural component of infectious
88 particles. It is not glycosylated and is likely derived from the assembly of the
89 intracellular ORF2 (ORF2intra) form present in the cytosolic compartment. Importantly,
90 we showed that a fraction of the ORF2intra form is translocated into the nucleus of
91 infected cells [13]. Nuclear localization of ORF2 was also described by Lenggenhager
92 *et al.* in naturally infected human hepatocytes [14], but the significance of ORF2
93 nuclear localization remains to be elucidated. The ORF2g and ORF2c proteins (herein
94 referred to as ORF2g/c) are highly glycosylated and secreted in large amounts in
95 culture supernatant (*i.e.,* about 1000x more than ORF2i [15]) and are the most
96 abundant antigens detected in patient sera [12]. These proteins likely act as a humoral
97 immune decoy that inhibits antibody-mediated neutralization [15]. How the different
98 forms of ORF2 are generated during the HEV lifecycle has not yet been fully
99 investigated. However, their sequence and post-translational modifications suggest
100 that they might be produced either by a distinct addressing into the secretory pathway
101 and the nucleus [12,13], and/or by a differential translation process[15].
102 Here we investigated the mechanisms by which the ORF2 forms are produced and
103 differentially addressed to cell compartments. We demonstrated that HEV has set up
104 a nucleo-cytoplasmic transport mechanism of its capsid protein to modulate cell host
105 immune responses. In addition, we found that during the HEV lifecycle, a fine-tuning
106 of ORF2 partitioning occurs between cytosolic, reticular and nuclear compartments.
107 Importantly, we identified a stretch of 5 amino acid residues (herein referred to as ARM,
108 Arginine-Rich Motif) in the N-terminal region of the ORF2 protein that drives nuclear
109 translocation and tightly modulates the stoichiometry between the different ORF2
110 forms, especially by regulating the functionality of the ORF2 signal peptide and
111 interactions with the host cell.

112 # Results

113

114 **The ORF2 protein transits through the nucleus in the early phase of infection.**

115 We and others previously showed that the ORF2 protein is translocated into the
116 nucleus of infected cells of patient liver biopsies [14] and in cell culture system [13].
117 Here, we first analyzed the ORF2 expression in PLC3 cells electroporated with the
118 infectious p6 strain (PLC3/HEV-p6), at different time post-electroporation (p.e.) by
119 immunofluorescence (**Fig 1**). ORF2 staining and quantification of nuclear fluorescence
120 showed that nuclear translocation of ORF2 takes place at early time points p.e. (*i.e.,*
121 18h) and is then followed by a nuclear export process, indicating that HEV has
122 developed mechanisms for ORF2 nuclear import and export.

123

124 **The ORF2 protein displays an Arginine-Rich Motif (ARM) that functions as a**
125 **Nuclear Localization Signal (NLS).**

126 To decipher the molecular mechanisms of ORF2 nuclear import, we first analyzed its
127 amino acid (aa) sequence with the NLSTradamus prediction program [16]. We
128 identified a potential Nuclear Localization Signal (NLS) corresponding to a conserved
129 Arginine-Rich Motif (ARM, 5 Arginine residues: RRRGRR) in the N-terminal region of
130 ORF2, downstream of its signal peptide (SP) (**Fig 2A**). We next generated a series of
131 ORF2 mutants in the p6 strain that are depicted in **Fig 2A**. We characterized their
132 expression and subcellular localization (**Figs 2B, 2C, S1** and **S2**), and their impact on
133 the HEV lifecycle (**Fig 2D**).

134 The replacement of arginine residues by alanine (3R/3A, 2R/2A and 5R/5A mutants)
135 led to a drastic reduction of ORF2 nuclear localization compared to the wt protein (**Figs**
136 **2B** and **2C**, Nuclear extract), indicating that the ARM is likely a functional NLS.

137 Interestingly, the reduced nuclear localization of these mutants was associated with an
138 accumulation of ORF2 in the Golgi apparatus (**S1 Fig**) and a reduced association with
139 cellular membranes (**Fig 2C**, Membrane extract), indicating that these mutated
140 proteins are likely soluble in the Golgi lumen. In addition, high molecular weight forms
141 of ORF2intra in the soluble fraction as well as an increase of ORF2g/c secretion were
142 observed (**Fig 2C**), suggesting a higher translocation into the secretory pathway
143 associated to an improved functionality of ORF2 SP. Quantification of intracellular
144 RNAs showed that replication was not altered in these mutants (**Fig 2D**). In addition,
145 ARM mutations did not affect ORF3 expression (**Fig 2C**). However, these mutants no
146 longer produced infectious viral progeny (**Fig 2D**). Thus, our results suggest that the
147 ARM drives the ORF2 nuclear translocation and plays important functions in the HEV
148 lifecycle, notably in the assembly of infectious particles.
149 We also generated mutants for which Pro25, Ser26 and Gly27 residues were replaced
150 by 3 arginine residues (PSG/3R mutant), and alternatively SP was fully or partially
151 deleted (ΔSP and ΔSP1 mutants, respectively) (**Fig 2A**). The PSG/3R mutant showed
152 a marked nuclear localization (**Figs 2B** and **2C**, Nuclear extract) but was impaired in
153 ORF2g/c secretion (**Fig 2C,** Supernatant), as observed for the SP deletion mutants,
154 indicating that the addition of arginine residues strengthens the NLS function of ARM
155 but inhibits the functionality of ORF2 SP. The PSG/3R mutant expressed the ORF3
156 protein but displayed lower intracellular replication levels and was no longer infectious
157 (**Fig 2D**). The increased nuclear localization of this mutant is therefore likely
158 responsible for the reduction of HEV RNA replication and assembly of infectious
159 particles.
160 The full (ΔSP) or partial (ΔSP1) deletion of the ORF2 SP led to a total inhibition of
161 ORF2 secretion (**Fig 2C**, Supernatant), as expected due to the absence of reticular

translocation. Interestingly, the ORF2 protein still exhibited a nuclear localization (**Fig 2B**), indicating that the nuclear translocation process is independent of the reticular translocation. Because ORF2 and ORF3 are overlapping, and ORF3 is essential to particle secretion, the SP deletion mutants did not express the ORF3 protein (**Fig 2C**) and displayed reduced extracellular titers (**Fig 2D**). Intracellular titers were also lowered in SP mutants (**Fig 2D**), indicating that the ORF2 SP likely plays an important role in the assembly of infectious particles.

Lastly, the highly conserved Gly31 residue was also mutated (**Fig 2A**, G/A mutant). This mutant displayed a subcellular distribution similar to that of wt, and expressed the ORF3 protein. Although to a lesser extent than wt, G/A mutant produced intracellular particles, but showed reduced extracellular RNA and infectious levels. This indicates that the G/A mutation affects particle secretion.

We next carried out a comparative study of NLS sequences in viral proteins and their importin. We found that the ORF2 ARM is similar to the Epstein-Barr nuclear antigen leader protein (EBNA-LP) arginine-rich NLS (RRVRRR) that interacts with Importin-α1 [17]. Interestingly, ORF2 and Importin-α1 co-localized in the nucleus of infected cells with a Pearson correlation coefficient (PCC) of 0.670, and the mutation of arginine residues drastically reduced this colocalization (**S2 Fig**).

Taken together, our results indicate that ORF2 colocalizes with Importin-α1 thanks to its ARM that serves as a functional NLS. In addition, these results suggest that the ARM is involved in the fine-tuning of the addressing and stoichiometry of the ORF2 protein between the nuclear, cytosolic and reticular pathways. This stoichiometry is likely essential to the HEV lifecycle.

187 **The nuclear translocation of ORF2 down-regulates the NF-κB-related signaling.**
188 Our results demonstrated that ORF2 localizes in the nucleus (ORF2ni) and the ARM
189 is pivotal for nuclear translocation. Our results also suggested that ORF2ni is readily
190 detected as early as 18 h.p.e. in PLC3/HEV-p6 cells while its nuclear targeting is
191 transient and starts to decrease after 48h (**Fig 1**). This observation prompted us to
192 address the impact of early nuclear translocation of ORF2 on the regulation of host
193 genes. We performed a transcriptomic analysis by microarrays (Agilent SurePrint
194 Technology) in PLC3/HEV-p6-wt, PLC3/HEV-p6-5R/5A, PLC3/HEV-p6-ΔORF3 and
195 PLC3 mock cells at 18 h.p.e. Interestingly, in PLC3/HEV-p6-wt and PLC3/HEV-p6-
196 ΔORF3 cells, we observed a significant inhibition of expression of 7 genes related to
197 the TNFα, IL-17 and NF-κB-mediated signaling as well as inflammatory responses
198 (*i.e.,* NOD-like receptor-induced response) (**Figs 2E** and **S3**). In contrast, no gene
199 expression inhibition was observed in PLC3/HEV-p6-5R/5A cells, reflecting the
200 significance of ORF2 nuclear translocation in the observed inhibition. Of note, while
201 some reports suggested that ORF3 expression modulates the host responses [18–23],
202 no marked difference was observed when comparing ΔORF3 mutant to wt.
203 Altogether our results suggest that the ORF2 ARM, which notably regulates ORF2
204 nuclear translocation, is a pivotal viral determinant for the modulation of host pathways
205 and, especially, genes of the NF-κB-induced signaling upon infection. Further studies
206 will be required to define precisely the impact of this HEV-driven host regulation on
207 immune cell responses.
208
209 **Nuclear export of the ORF2 protein**
210 The observation that ORF2 nuclear targeting is transient and decreases after 48h (**Fig**
211 **1**) then prompted us to investigate the mechanisms of ORF2 nuclear export. We

212 treated PLC3/HEV-p6 cells with nuclear export inhibitors, Leptomycin B (LepB) and
213 Verdinexor (Verd). These compounds are irreversible (LepB) and reversible (Verd)
214 inhibitors of the ubiquitous transport receptor chromosome maintenance protein 1
215 (CRM1/Exportin 1), which recognizes hydrophobic leucine-rich export signals [24].
216 Treated cells displayed a highly significant nuclear accumulation of ORF2, as
217 compared to control cells (**Fig 3A**). In addition, co-localization studies revealed that
218 ORF2 partially or transiently colocalizes with CRM1 in untreated cells whereas they
219 significantly colocalize upon treatment with nuclear export inhibitors (**S4 Fig**). These
220 results indicate that ORF2 undergoes a nuclear export to the cytoplasm by a CRM1-
221 dependent mechanism.
222 CRM1 recognizes hydrophobic leucine-rich export signals. By analyzing the ORF2
223 sequence, we identified at least 12 potential nuclear export signals (NES) into the
224 ORF2 sequence. We replaced the hydrophobic residues in these conserved motifs by
225 alanine residues and characterized the generated mutants as described above. Most
226 of mutations did not affect ORF2 partitioning, whereas three mutants named NES9,
227 NES10 and NES12 (**Fig 3B**) led to a highly significant accumulation of ORF2 inside
228 the nucleus (**Figs 3C** and **3D**), as observed for cells treated with nuclear export
229 inhibitors (**Fig 3A**). NES9 and NES10 mutants were no longer infectious, whereas the
230 NES12 mutant with the lowest nuclear accumulation (**Fig 3C**) still exhibited some
231 intracellular and extracellular infectivity (**Fig 3E**). Of note, intracellular replication was
232 not altered by NES mutations (**Fig 3F**), indicating that the loss of infectious particle
233 assembly is due to the differential subcellular localization of the mutants and not to a
234 replication defect.
235 These results indicate that HEV has set up a nuclear export system for its ORF2 capsid
236 protein. This mechanism involves CRM1 which recognizes three NES on the ORF2

237 sequence. Moreover, these results suggest again that a fine balance between the
238 nuclear, cytosolic and reticular pathways is likely essential to the HEV lifecycle.
239

240 **Translocation and maturation of the glycosylated ORF2 forms**

241 Next, we investigated the mechanisms of translocation and maturation of the highly
242 secreted and glycosylated ORF2g/c isoforms. First, we treated PLC3/HEV-p6 and
243 Mock cells with Mycolactone, an inhibitor of Sec61 translocon, the membrane
244 embedded protein complex responsible for the translocation of newly synthetized
245 polypeptides into the ER lumen [25]. Interestingly, we observed a dose-dependent
246 reduction of ORF2g/c secretion in Mycolactone-treated PLC3/HEV-p6 cell
247 supernatants (**Fig 4A**), indicating that reticular translocation of the ORF2g/c forms is
248 Sec61-dependent.

249 Previously, we demonstrated that the first residues of ORF2i, ORF2g and ORF2c
250 proteins are Leu14, Ser34 and Ser102, respectively [12,13] (**Fig 3B**). Therefore, the
251 first 20 aa of the ORF2i protein are not present in the ORF2g/c isoforms. Furthermore,
252 the ORF2i protein is not glycosylated whereas ORF2g/c proteins are highly
253 glycosylated [13] (**Fig 4B**). Thanks to these features, we generated a murine
254 monoclonal antibody (P1H1) that recognizes the N-terminus of ORF2i (**Fig 4B**). P1H1
255 specifically immunoprecipitates the ORF2i protein without cross-reacting with the
256 highly secreted and glycosylated ORF2g/c proteins (**Fig 4C**, SN). We also generated
257 the P3H2 antibody that recognizes the different isoforms of ORF2. Both antibodies
258 recognize the intracellular ORF2 form (**Fig 4C,** Cells).

259 These antibodies were used to evaluate the effects of three furin inhibitors and related
260 proprotein convertases (PC) on ORF2g/c maturation. PC cleave the multibasic motifs
261 R/K-X_n-R/K (where X_n corresponds to a 0-, 2-, 4-, 6-amino-acid spacer) in the precursor

262 proteins[26]. The presence of ARM and RRR motif upstream of the ORF2g/c N-termini
263 (**Fig 3B**), respectively, suggests that a PC might be involved in the maturation of these
264 ORF2 forms. Therefore, we treated PLC3/HEV-p6 cells with three potent furin/PC
265 inhibitors (decanoyl-RVKR-chloromethylketone [CMK], hexa-D-arginine amide [D6R],
266 and SSM3 trifluoroacetate [SSM3]) [27] and immunoprecipitated ORF2 proteins in cell
267 supernatants with P1H1 and P3H2 antibodies. Intracellular contents were probed by
268 WB for ORF2intra, cleavage of cellular αV-pro-integrin (a substrate of intracellular
269 furin) and tubulin (**Figs 4D-F**). In these experiments, immunoprecipitation of ORF2g by
270 P1H1 antibody was used as a read-out of the inhibition of ORF2g maturation (**Fig 4B,**
271 ORF2g*). In treated cells, we observed a dose-dependent immunoprecipitation of
272 ORF2g* by P1H1 (**Figs 4D-F**), indicating that furin/PC inhibitors abrogated ORF2g
273 maturation. Of note, the cell-permeable CMK and SSM3 inhibitors showed a strong
274 inhibition of ORF2g and αV-pro-integrin maturation, whereas the cell membrane
275 impermeable D6R inhibitor showed a moderate effect on ORF2g maturation. Together,
276 these results indicate that a furin/PC present in the secretory pathway is likely involved
277 in the ORF2g/c maturation process.
278
279 **The ORF2 ARM is the regulator of ORF2 addressing**
280 To further analyze the molecular mechanisms by which ORF2 is differentially
281 addressed to the cytosolic, nuclear or reticular pathways, we next generated chimeric
282 and mutant constructs between ORF2 and the CD4 glycoprotein, as a reporter protein.
283 Therefore, we used a heterologous expression system for the further experiments. The
284 constructs were expressed in Huh-7 cells stably expressing the T7 RNA-polymerase
285 (H7-T7-IZ cells) [28]. We selected the 5R/5A and PSG/3R mutations for their marked
286 phenotype (**Fig 2**) and generated an ARM-deleted mutant (ΔARM, deletion of Gln24

287 to Arg33, **Fig 5**). The full-length ORF2wt, ORF2$^{5R/5A}$ and ORF2$^{PSG/3R}$ proteins displayed
288 a similar pattern and phenotype as observed in the infectious system (**Fig 2**), by
289 immunofluorescence and WB (**Fig 5**). The effect of the 5R/5A mutation or the ARM
290 deletion on the ORF2 secretion, membrane association and nuclear localization
291 confirmed that the ARM located downstream of the SP negatively regulates ORF2
292 reticular translocation but is important for nuclear translocation and membrane
293 association. Conversely, the PSG/3R mutation showed an increased nuclear
294 localization and membrane association, whereas ORF2 secretion was fully blocked,
295 confirming that positively charged residues negatively regulate the functionality of
296 ORF2 SP but mediate nuclear translocation and membrane association.
297 Next, to define the impact of ARM on another SP, we exchanged the ORF2 SP by the
298 one of CD4 that is a functional model SP [29] (**Fig 5,** Chimeras C1). Interestingly, the
299 chimera C1 displayed a subcellular distribution similar to that of ORF2wt but was no
300 longer secreted (**Fig 5C**, SN), indicating that the ARM inhibits the functionality of CD4
301 SP. Indeed, the mutation (C1$^{5R/5A}$) or deletion of ARM (C1$^{\Delta ARM}$) restored secretion of
302 the chimera C1. The observation that ORF2wt is secreted in the presence of the ARM
303 whereas it is not with the CD4 SP, suggests the existence of an interplay between
304 ORF2 SP and ARM. The chimera C1$^{PSG/3R}$ showed an increased nuclear localization
305 and membrane association, whereas its secretion was abolished (**Fig 5**), confirming
306 that positively charged residues downregulate the functionality of CD4 SP and mediate
307 nuclear translocation and membrane association. It should be noted that the chimera
308 C1$^{PSG/3R}$ showed a marked reticular staining (**Fig 5A**). As described below, we
309 hypothesized that the CD4 SP might disturb the maturation of ORF2i and anchors the
310 protein into the membrane on the cytosolic side.

311 We also generated an additional group of ORF2 constructs in which the SP of ORF2
312 was partially deleted (C2) (**S5 Fig**). The characterization of these constructs confirmed
313 that ARM mediates ORF2 nuclear translocation and membrane association
314 independently of the reticular translocation.
315 In order to specifically study the impact of ARM on the functionality of the ORF2 SP
316 independently of the ORF2 ectodomain, CD4 chimeras containing the SP ($CD4^{SPORF2}$),
317 the N-terminus (Chimeras C4) or the ARM of ORF2 (Chimeras C5) were also
318 generated and characterized as previously (**Fig 6**). Thanks to the $CD4^{SPORF2}$ construct,
319 we confirmed that the SP of ORF2 is a functional SP, as illustrated by its subcellular
320 pattern (**Fig 6A**) and its efficient secretion (**Fig 6D**). Interestingly, the chimera C4
321 showed an intracellular distribution different from that of CD4wt, with a significant
322 nuclear localization (**Figs 6A** and **6B**). In addition, WB analysis revealed a major
323 decrease in C4 secretion as well as the appearance of a 40kDa band in the soluble
324 fraction (**Fig 6D**). This band corresponds to the non-N-glycosylated CD4 ectodomain,
325 which contains 2 N-glycosylation sites, indicating that the CD4 ectodomain is poorly
326 translocated into the ER lumen when fused to ORF2 N-terminus. The same
327 observations were made for the chimera $C4^{PSG/3R}$. In contrast, the 5R/5A mutations
328 restored the secretion but abolished the nuclear translocation of C4 ($C4^{5R/5A}$, **Figs 6A**,
329 **B** and **D**). Characterization of the chimeras C5, which contain only the ORF2 ARM,
330 showed results similar to the chimeras C4 (**Figs 6B-D)**. However, unlike C4, the
331 chimera C5 was no longer secreted (**Fig 6D)**, supporting the hypothesis of an interplay
332 between ORF2 SP and ARM. Moreover, the chimera C5 displayed a reticular staining
333 in addition to nuclear staining (**Fig 6C)**. This observation is in line with our hypothesis
334 that the CD4 SP does not undergo the same maturation as ORF2 SP, and anchors the
335 protein into the membrane with a cytosolic orientation.

336 Taken together, these results demonstrate that the ORF2 ARM on its own is capable
337 of regulating the functionality of ORF2 or CD4 SP, as well as the nuclear translocation
338 of the protein that carries it.
339
340 **The ORF2 ARM regulates the topology of ORF2 SP**
341 Positively charged residues, such as arginine residues, are known to function as
342 determinants of membrane protein topology, which is reflected in a statistical rule of
343 membrane topology, *i.e.* the positive-inside rule of membrane proteins [30]. Notably,
344 positive charges determine the orientation of the signal sequences and contribute to
345 membrane spanning of the SP H-segment translocating through the translocon [30].
346 Since our results suggest that the ARM regulates the SP functionality and membrane
347 association of ORF2, we next analyzed the topology of our different ORF2 and CD4
348 constructs by immunofluorescence (**Figs 7** and **8**). We used a low concentration of
349 digitonin that selectively permeabilizes the plasma membrane. Triton X-100-
350 permeabilized cells were analyzed in parallel as a control. The differential detection of
351 two epitopes on the ER-membrane associated Calnexin (CNX) was used as a control
352 of permeabilization. We observed that the ORF2wt, the chimera C1 and the PSG/3R
353 mutants displayed a staining in both Triton X-100 and Digitonin-permeabilized cells
354 whereas the ΔARM and 5R/5A constructs showed a labelling only in Triton X-100
355 permeabilized cells (**Fig 7**). These accessibility differences in association with the
356 secretion efficiencies (**Figs 5C** and **6D**), which reflect the reticular translocation,
357 allowed us to infer the membrane orientation of each construct as well as the SP
358 topology (**Figs 7** and **8**). Thus, in the presence of the ARM, the ORF2 SP likely adopts
359 a double topology (ORF2wt) whereas the CD4 SP is not functional (C1) and sticks the
360 protein to the cytosolic side of membranes. The ORF2 SP and CD4 SP are fully

361 functional when the ARM is deleted (ΔARM) or mutated (5R/5A) whereas they are
362 nonfunctional when the ARM is coupled to the PSG/3R mutations. The same
363 observations were done for the C4 and C5 chimeras (**Fig 8**).
364 Thus, our findings demonstrate that the ORF2 SP and the ARM act together to direct
365 the fate of ORF2 capsid protein. Thanks to the ARM, the ORF2 SP is likely able to
366 adopt a dual topology leading to either reticular translocation or membrane integration
367 to the cytosolic side.
368

369 # Discussion

370 In the present study, we analyzed a series of mutants of the HEV ORF2 capsid protein
371 to gain insight into how a same primary sequence can generate several ORF2 isoforms
372 with distinctive sequences, post-translational modifications, subcellular localizations
373 and functions in the HEV lifecycle. Several important conclusions can be drawn from
374 our analyses. The first is that the ORF2 protein early transits through the nucleus
375 during infection to control specific cellular functions *i.e.* antiviral responses of the
376 infected cell. We identified the determinants of the ORF2 nuclear import and export.
377 Notably, an ARM in the N-terminal region of ORF2 mediates nuclear import.
378 Importantly, we showed that the mutation of this motif abolishes ORF2 nuclear
379 translocation but also affects ORF2 addressing into membrane, cytosolic and reticular
380 compartments, which was deleterious for the HEV lifecycle. This brings us to the
381 second important finding, the ARM is pivotal in the fine-tuning of the partitioning and
382 stoichiometry of the ORF2 protein between the nuclear, cytosolic and reticular
383 pathways that are essential to the HEV lifecycle. The last significant finding in this study
384 is the manner by which the SP and ARM cooperate to control the fate of ORF2 protein.
385 Indeed, in addition to mediate the targeting of ORF2 to the ER membrane, the SP is
386 likely able to adopt a reverse signal-anchor topology. This topology inversion would be
387 driven by flanking charged residues of ARM according to the positive-inside rule
388 [31,32] and leads to the anchoring of the ORF2i protein to the cytosolic side of
389 membranes.
390
391 Previously, we [12] and others [15] demonstrated that HEV produces several isoforms
392 of the ORF2 capsid protein. The ORF2i protein is the structural component of infectious
393 particles. It is likely derived from the assembly of the ORF2intra form present in the

394 cytosolic compartment. The ORF2i and ORF2intra proteins are not glycosylated and
395 display the same sequence starting at Leu14 corresponding to the middle of the SP,
396 indicating that an intra-membrane protease might be involved in their maturation.
397 Further investigation is required to identify this intramembrane protease. In contrast,
398 ORF2g/c proteins are highly glycosylated and secreted, but are not associated with
399 infectious material. We identified the first residues of ORF2g/c as Ser34 and Ser102,
400 respectively [12,13]. The nature of the sequences upstream of the ORF2g/c N-termini
401 and our experiments using PC inhibitors, suggest that a PC, such as Furin, might be
402 involved in their maturation[33]. Intriguingly, the ARM is right upstream of the N-
403 terminus of ORF2g, indicating that this motif also serves as recognition site for ORF2g
404 maturation. Further experiments are needed to thoroughly investigate the processing
405 of ORF2 forms.
406
407 We demonstrated that early during infection, the ORF2 protein transits through the
408 nucleus likely to control antiviral responses of the infected cell. Although we identified
409 the determinants of nuclear import and export in the ORF2 sequence, further studies
410 are now required to identify the cellular partners of nuclear ORF2 and define precisely
411 the impact of ORF2 host regulation on immune cell responses. A previous study
412 demonstrated the significance of ORF2 N-terminal Arginine residues in the inhibition
413 of TBK1-mediated IRF3 phosphorylation [34] Although they did not take into account
414 the effect of Arginine residues on ORF2 partitioning, their results are in line with our
415 observations on ORF2 interference with the host innate immunity.
416
417 Based on our findings, we propose a model of ORF2 production. Firstly, when engaged
418 with the translocon, the ORF2 SP initially inserts head-on in an N_{exo}/C_{cyt} orientation

419 (**Fig 9A**). Two mechanisms can then take place. In one side, ORF2 SP inverts
420 orientation to N_{cyt}/C_{exo} to integrate the ER membrane as cleavable signal. The C-
421 terminal end of signal is exposed to the ER lumen and cleaved by signal peptidase,
422 liberating the ORF2 ectodomain in the ER lumen where it undergoes glycosylation and
423 protease maturation. This pathway leads to the production of ORF2g/c proteins that
424 are abundantly secreted and likely serve as immunological baits (**Fig 9B**). On the other
425 side, ORF2 SP does not invert, keeps a N_{exo}/C_{cyt} orientation and serves as a reverse
426 signal anchor. Next, the ORF2 protein anchored to the cytosolic side of membranes is
427 likely processed by an intramembrane protease (**Fig 9C**). This pathway leads to the
428 production of the ORF2intra protein that is early translocated into the nucleus to play
429 immunomodulatory functions and/or is then assembled into viral particles in the
430 cytosolic compartment. Of note, the dual topology was exclusively observed for the
431 ORF2 and CD4 constructs containing both ORF2 SP and ARM (ORF2wt and chimera
432 C4), reflecting the specific interplay between ORF2 SP and ARM and no involvement
433 of other sequence determinant in this process.
434
435 Due to the size constraint of their extracellular phase, viruses are under strong
436 pressure to minimize the size of their genome. Overlapping genes represent an
437 adaptive strategy developed by many viruses to condense a maximum amount of
438 information into short nucleotide sequences. This gene overlap strategy is used by
439 HEV for the ORF2 and ORF3 expression[35] and ORF4 in gt1 [36]. Here, our study
440 enabled the pioneering demonstration that HEV also developed a master strategy to
441 condense multiple information into only five amino acids of its capsid protein. This
442 strategy is likely also exploited by other pathogens. Thus, the ORF2 ARM is a central
443 regulator of the HEV lifecycle that controls (i) the ORF2 nuclear localization and hereby

444 controls cellular functions promoting regulation of host antiviral responses, (ii) the
445 functionality of ORF2 SP leading to the production of either viral particles or humoral
446 immune decoys, (iii) maturation of glycosylated ORF2 protein by cellular proteases,
447 and (iv) membrane association that is likely essential to particle assembly. Hence,
448 ARM controls the fate and function of ORF2 capsid protein isoforms and is likely a key
449 player in the hijacking of cellular processes.
450

451 # Materials and Methods

452 **Cell cultures.** PLC3 [12]and Huh-7.5 [37] cells were cultured as previously described
453 [13]. The Huh-7-derived H7-T7-IZ cells stably expressing the T7 RNA polymerase
454 ([28]; kindly provided by Ralf Bartenschlager, University of Heidelberg, Germany) were
455 maintained in a medium supplemented with 50 µg/ml of Zeocin. They were used for
456 the transfection of the T7 promoter-driven pTM expression vectors.
457
458 **Plasmids and transfection.** The plasmid pBlueScript SK(+) carrying the DNA of the
459 full length genome of adapted gt3 Kernow C-1 p6 strain, (GenBank accession number
460 JQ679013, kindly provided by S.U Emerson) was used as a template[11]. Mutants of
461 the ORF2 ARM or NES sites were generated by site directed mutagenesis. Individual
462 mutations were introduced by sequential PCR steps, as described previously [13],
463 using the Q5 High-Fidelity 2X Master Mix (New England Biolabs, NEB), then digestions
464 with restriction enzymes and ligation were performed. All the mutations were verified
465 by DNA sequencing. The primers used for the generation of ORF2 mutants are listed
466 in **S1 Table.** The ORF3-null mutant of HEV-p6 (HEV-p6-ΔORF3) was generated as
467 described in [38]
468 Capped genomic HEV RNAs were prepared with the mMESSAGE mMACHINE kit
469 (Ambion) and delivered to PLC3 cells by electroporation using a Gene Pulser Xcell™
470 apparatus (Bio-Rad) [12].
471 The plasmids pTM-ORF2 (kindly provided by J. Gouttenoire, University of Lausanne,
472 Switzerland) [14] and pTM/CD4 have been previously described [14,39]. The
473 pTM/CD4 contains the DNA sequence coding for the secreted ectodomain of CD4 (aa
474 1-371). The primers used for the generation of ORF2/CD4 chimeras/mutants are listed
475 in **S1 Table.** For some constructs, PCR amplifications were performed by multiple heat

476 pulses [40]. The pTM plasmids were transfected into H7-T7-IZ cells using ViaFect™
477 Transfection Reagent (Promega) following the manufacturer's recommendations.
478
479 **Antibodies.** Primary antibodies used in this study are listed in **Table 1**. Secondary
480 antibodies were from Jackson ImmunoResearch.
481
482 **Table 1: Primary antibodies used for Western-blot and indirect**
483 **immunofluorescence experiments.**
484

Target	Clone / Species / Isotype	Reference	Supplier	Antibody registry reference
HEV ORF2	1E6 / Mouse / IgG2b	MAB8002	Millipore	AB-827236
HEV ORF2	P1H1 / Mouse / IgG3	Patent # PCT/EP2019/068338	Home-made	x
HEV ORF2	P3H2 / Mouse / IgG3	Unpublished	Home-made	x
HEV ORF3	Rabbit	Graff *et al.* [38]	Gift of S. Emerson (NIH)	x
CD4	Rabbit	ab133616	Abcam	AB-270883
Importin α-1	Goat	ab6036	Abcam	AB-30524
CRM1	Rabbit	#46249	Cell Signaling	AB-2799298
γ-Tubulin	Mouse / IgG1	#T-5326	Sigma-Aldrich	AB-532292
CNX-N	Rabbit mAb	ab92573	Abcam	AB-10563673
CNX-C	Rabbit	ab22595	Abcam	AB-2069006
SP1	Rabbit	#PA5-29165	Thermofisher	AB-2546641
GM130	Mouse / IgG1	#610822	BD Biosciences	AB-398141
Lamin B1	Rabbit	ab16048	Abcam	AB-443298
αV-integrin	Rabbit	ab124968	Abcam	AB-11129746

485
486
487 **Indirect immunofluorescence.** Immunostainings were performed as previously
488 described [13]For selective permeabilization experiments, cells were fixed with 2% of
489 PFA, washed twice with PBS and permeabilized for 30 min at 4°C with either 0.01% of
490 Digitonin (Sigma) in buffer containing 20 mM HEPES pH6.9, 0.3 M sucrose, 0.1 M KCl,
491 2.5 mM MgCl2 and 1 mM EDTA or 0.5% Triton X-100 in PBS. Cells were next stained
492 with buffers containing Digitonin.

493 The nuclei were stained with DAPI and cell outlines with CellMask^{TM} Green
494 (Invitrogen). Cells were analyzed with a LSM 880 confocal laser-scanning microscope
495 (Zeiss) using Plan Apochromat 63xOil/1.4N.A. and EC Plan Neofluar 40xOil/1.4N.A.
496 objectives. The images were processed using ImageJ and Fiji softwares.
497
498 **Quantification of the ORF2 protein nuclear fluorescence.** The method was adapted
499 from McCloy *et al*. [41]. Briefly, the ORF2 protein nuclear fluorescence was determined
500 using the ImageJ software. The regions of interest (ROI) were drawn around cell
501 nuclei. Area, integrated density and mean gray values were measured. Then,
502 corrected total cell fluorescence (CTCF) was calculated by the following formula: CTCF
503 = integrated density – (area of selected electroporated cells x mean of background
504 fluorescence around the cells). The exact nuclear fluorescence was = CTCF-the mean
505 of the integrated density of non-infected cells.
506 For nuclear/cytosolic fluorescence intensity ratio, cells were co-stained with
507 CellMask^{TM} Green (Invitrogen) and analyzed using ImageJ software. ROI were drawn
508 around the whole cells and the nuclei. Area, integrated density, mean values and the
509 exact cell and nuclear fluorescence were measured and calculated as described
510 above. For each cell, the nuclear/cytosolic fluorescence intensity ratio was calculated
511 by the following formula: exact fluorescence intensity of nucleus / (exact fluorescence
512 intensity of whole cell - exact fluorescence intensity of nucleus).
513
514 **Pearson's correlation coefficient (PCC) determination.** Colocalization studies were
515 performed by calculating the PCC using the JACoP plugin of ImageJ software. For
516 each calculation, at least 30 cells were analyzed.
517

518 **Virus production and intracellular viral particles preparation.** PLC3 cells were
519 electroporated with HEV-p6 RNAs as previously described [12]. Intracellular viral
520 particles were prepared by osmotic shock, as previously described [13]
521
522 **Infectious titer determination.** Infectious titers in focus forming unit (FFU/mL) were
523 determined as described previously [13] by using Huh7.5 cells. ORF2-positive cells
524 were quantified using an InCell 6000 confocal analyzer (GE Healthcare) and the
525 Columbus image analysis software (Perkin Elmer).
526
527 **Chemicals and Viability assay.** Leptomycin B (Cell Signaling), Verdinexor (AdooQ®
528 Biosciences), Mycolactone A/B toxin [42]Decanoyl-RVKR-chloromethylketone [CMK]
529 (Sigma), hexa-D-arginine amide [D6R] (Sigma) and SSM3 trifluoroacetate (Tocris)
530 were used in this study. Dose-response curves of PLC3 cells treated with the different
531 drugs are shown in **S6 Fig.** Cell viability was assessed using a CellTiter 96® AQueous
532 Non-Radioactive Cell Proliferation Assay (Promega).
533
534 **RNA extraction and quantification.** HEV RNA and cellular gene RNA levels were
535 quantified by RT-qPCR as described in **Supporting Information**.
536
537 **Western blotting analysis.** Western blotting analyses were performed as described
538 previously [12]. Target proteins were detected with specific antibodies (**Table 1**) and
539 corresponding peroxidase-conjugated secondary antibodies.

540 **Immunoprecipitations.** P1H1 and P3H2 antibodies were bound to magnetic
541 Dynabeads® M-270 Epoxy beads (Thermofisher) overnight at 37°C following the
542 manufacturer's recommendations. Beads were washed and then incubated for 1h at

543 RT with heat-inactivated supernatants. Beads were washed and then heated at 80°C
544 for 20 min in Laemmli buffer. Proteins were separated by SDS-PAGE and ORF2
545 proteins were detected by WB using the 1E6 MAb.

546 **Subcellular extraction.** Extractions were performed with the Subcellular Protein
547 Fractionation Kit for Cultured Cells (Thermo scientific) following the manufacturer's
548 recommendations. The cytoplasmic extracts were ultra-centrifugated at 100 000 g
549 during 1h at 4°C. Anti-β-tubulin (cytoplasmic), anti-Calnexin (membranous) and anti-
550 SP1 or anti-Lamin B1 (nuclear soluble) antibodies were used to control the quality of
551 extractions.
552

553 **Transcriptomic analysis.** Gene expression analysis was performed at 18 h.p.e. on
554 PLC3 cells electroporated with HEV-p6-wt, HEV-p6-5R/5A, HEV-p6-ΔORF3 RNAs or
555 no RNA (mock). Oligonucleotide microarrays for human whole genome (G4858A
556 design 072363, 8x60k chips SurePrint G3 unrestricted GE, Agilent Technologies) were
557 used for global gene expression analysis, as described in **Supporting Information**.
558

559 **Statistical analyses.** Statistical analyses were performed with the software RStudio
560 version 1.2.5001 combined with R version 3.6.1. For all statistical tests, reported p
561 values were two-sided. A test was declared statistically significant for any p value
562 below 0.05. For comparing more than three groups of unpaired data, ANOVA or its
563 non-parametric equivalent test, the Kruskal-Wallis test, was used. ANOVA was
564 preferred when the distributions in each group followed a normal distribution, and the
565 assumption of equality of the variances between each group was verified. When tests
566 showed a significant difference between the groups, post hoc tests were performed.

567 The Dunnett test (dunnettTest function with default option) followed an ANOVA, and
568 the Conover's test (kwManyOneConoverTest function with pvalues adjusted by the
569 Benjamini-Hochberg procedure) followed the Kruskal-Wallis test. Each group was
570 compared to a reference. For the kinetic experiment, the Friedman test was preferred
571 because of a lack of normality and homogeneity of variance. The post hoc Nemenyi
572 test (frdManyOneNemenyiTest function from the package PMCMRplus) was used and
573 each time point was compared to data observed at 18 h.p.e.

574

Acknowledgments

This work was supported by a grant from the French agency ANRS-Maladies infectieuses émergentes. This work was also supported by the Pasteur Institute of Lille, Région Hauts-de-France and Inserm-transfert. K.H., M.A. and T.V. were supported by a fellowship from the ANRS. M.F. was supported by a fellowship from the Pasteur Institute of Lille and Région Hauts-de-France. The PLBS platform used in this work was supported by the ANR (ANR-10-EQPX-04-01) and Feder (12001407 [D-AL] EquipEx ImagInEx BioMed). We thank Olivia Beseme for her technical contribution. We thank Suzanne U. Emerson (NIH, USA), Jérôme Gouttenoire (University of Lausanne) and Ralph Bartenschlager (University of Heidelberg) for providing us with reagents. We thank François-Loïc Cosset (University of Lyon) for critical reading of the manuscript.

Author Contributions

K.H., M.F., M.A., C.M., C.C., V.A., A.D., C.L., A.T.F., P.B., D.H., T.V., J-M.S., S.S-D., A.V., P.B., M.D., Y.R., J.D., C-M.A., and L.C. performed research and/or analyzed data.

L.M., M.D., Y.R. contributed to reagents or analytic tool.

L.C. wrote the paper.

Declaration of Interests

The authors declare no competing interests.

599 # References

600

601 1. Horvatits T, Wiesch JS zur, Lütgehetmann M, Lohse AW, Pischke S. The Clinical
602 Perspective on Hepatitis E. Viruses. 2019;11: 617–19. doi:10.3390/v11070617

603 2. Wang S, Cheng X, Dai X, Dong C, Xu M, Liang J, et al. Rabbit and human
604 hepatitis E virus strains belong to a single serotype. Virus research. 2013;176: 101–
605 106. doi:10.1016/j.virusres.2013.05.013

606 3. Doceul V, Bagdassarian E, Demange A, Pavio N. Zoonotic Hepatitis E Virus:
607 Classification, Animal Reservoirs and Transmission Routes. Viruses. 2016;8: 270.
608 doi:10.3390/v8100270

609 4. Feng Z, Hensley L, McKnight KL, Hu F, Madden V, Ping L, et al. A pathogenic
610 picornavirus acquires an envelope by hijacking cellular membranes. Nature.
611 2013;496: 367–371. doi:10.1038/nature12029

612 5. Yin X, Li X, Feng Z. Role of Envelopment in the HEV Life Cycle. Viruses. 2016;8.
613 doi:10.3390/v8080229

614 6. Tam AW, Smith MM, Guerra ME, Huang CC, Bradley DW, Fry KE, et al. Hepatitis
615 E virus (HEV): molecular cloning and sequencing of the full-length viral genome.
616 Virology. 1991;185: 120–131.

617 7. LeDesma R, Nimgaonkar I, Ploss A. Hepatitis E Virus Replication. Viruses.
618 2019;11: 719–17. doi:10.3390/v11080719

619 8. Nimgaonkar I, Ding Q, Schwartz RE, Ploss A. Hepatitis E virus: advances and
620 challenges. Nat. Rev. Gastroenterol. Hepatol. 2018;15: 96–110.
621 doi:10.1038/nrgastro.2017.150

622 9. Yang Y-L, Nan Y-C. Open reading frame 3 protein of hepatitis E virus: Multi-
623 function protein with endless potential. World J Gastroentero. 2021;27: 2458–2473.
624 doi:10.3748/wjg.v27.i20.2458

625 10. Wißing MH, Brüggemann Y, Steinmann E, Todt D. Virus–Host Cell Interplay
626 during Hepatitis E Virus Infection. Trends Microbiol. 2020;29: 309–319.
627 doi:10.1016/j.tim.2020.07.002

628 11. Shukla P, Nguyen HT, Faulk K, Mather K, Torian U, Engle RE, et al. Adaptation
629 of a genotype 3 hepatitis E virus to efficient growth in cell culture depends on an
630 inserted human gene segment acquired by recombination. J Virol. 2012;86: 5697–
631 5707. doi:10.1128/jvi.00146-12

632 12. Montpellier C, Wychowski C, Sayed IM, Meunier J-C, Saliou J-M, Ankavay M, et
633 al. Hepatitis E Virus Lifecycle and Identification of 3 Forms of the ORF2 Capsid
634 Protein. Gastroenterology. 2018;154: 211-223.e8. doi:10.1053/j.gastro.2017.09.020

635 13. Ankavay M, Montpellier C, Sayed IM, Saliou J-M, Wychowski C, Saas L, et al.
636 New insights into the ORF2 capsid protein, a key player of the hepatitis E virus
637 lifecycle. Sci Rep. 2019;9: 6243. doi:10.1038/s41598-019-42737-2

638 14. Lenggenhager D, Gouttenoire J, Malehmir M, Bawohl M, Honcharova-Biletska H,
639 Kreutzer S, et al. Visualization of hepatitis E virus RNA and proteins in the human
640 liver. J Hepatol 2017;67: 471–479. doi:10.1016/j.jhep.2017.04.002

641 15. Yin X, Ying D, Lhomme S, Tang Z, Walker CM, Xia N, et al. Origin, antigenicity,
642 and function of a secreted form of ORF2 in hepatitis E virus infection. Proc Natl Acad
643 Sci USA 2018;3: 201721345–6. doi:10.1073/pnas.1721345115

644 16. Ba ANN, Pogoutse A, Provart N, Moses AM. NLStradamus: a simple Hidden
645 Markov Model for nuclear localization signal prediction. BMC Bioinformatics.
646 2009;10: 202. doi:10.1186/1471-2105-10-202

647 17. Nakada R, Matsuura Y. Crystal structure of importin-α bound to the nuclear
648 localization signal of Epstein-Barr virus EBNA-LP protein. Protein Science. 2017;26:
649 1231–1235. doi:10.1002/pro.3173

650 18. Dong C, Zafrullah M, Mixson-Hayden T, Dai X, Liang J, Meng J, et al.
651 Suppression of interferon-α signaling by hepatitis E virus. Hepatology. 2012;55:
652 1324–1332. doi:10.1002/hep.25530

653 19. Lei Q, Li L, Zhang S, Li T, Zhang X, Ding X, et al. HEV ORF3 downregulates
654 TLR7 to inhibit the generation of type I interferon via impairment of multiple signaling
655 pathways. Sci Rep. 2018;8: 1–10. doi:10.1038/s41598-018-26975-4

656 20. Wang M, Huang Y, He M, Peng W-J, Tian D-Y. Effects of hepatitis E virus
657 infection on interferon production via ISG15. World J Gastroentero. 2018;24: 2173–
658 2180. doi:10.3748/wjg.v24.i20.2173

659 21. He M, Wang M, Huang Y, Peng W, Zheng Z, Xia N, et al. The ORF3 Protein of
660 Genotype 1 Hepatitis E Virus Suppresses TLR3-induced NF-κB Signaling via TRADD
661 and RIP1. Sci Rep. 2016; 1–13. doi:10.1038/srep27597

662 22. Nan Y, Ma Z, Wang R, Yu Y, Kannan H, Fredericksen B, et al. Enhancement of
663 Interferon Induction by ORF3 Product of Hepatitis E Virus. J Virol. 2014;88: 8696–
664 8705. doi:10.1128/jvi.01228-14

665 23. Xu J, Wu F, Tian D, Wang J, Zheng Z, Xia N. Open reading frame 3 of genotype
666 1 hepatitis E virus inhibits nuclear factor-κappa B signaling induced by tumor
667 necrosis factor-α in human A549 lung epithelial cells. PLoS ONE. 2014;9: e100787.
668 doi:10.1371/journal.pone.0100787

669 24. Mathew C, Ghildyal R. CRM1 Inhibitors for Antiviral Therapy. Front Microbiol
670 2017;8: 10995–20. doi:10.3389/fmicb.2017.01171

671 25. Demangel C, High S. Sec61 blockade by mycolactone: A central mechanism in
672 Buruli ulcer disease. Biology of the cell / under the auspices of the European Cell
673 Biology Organization. 2018;110: 237–248. doi:10.1111/boc.201800030

674 26. Seidah NG, Prat A. The biology and therapeutic targeting of the proprotein
675 convertases. Nat Rev Drug Discov. 2012;11: 367–383. doi:10.1038/nrd3699

676 27. Cheng Y-W, Chao T-L, Li C-L, Chiu M-F, Kao H-C, Wang S-H, et al. Furin
677 Inhibitors Block SARS-CoV-2 Spike Protein Cleavage to Suppress Virus Production
678 and Cytopathic Effects. Cell Reports. 2020;33: 108254.
679 doi:10.1016/j.celrep.2020.108254

680 28. Romero-Brey I, Merz A, Chiramel A, Lee J-Y, Chlanda P, Haselman U, et al.
681 Three-dimensional architecture and biogenesis of membrane structures associated
682 with hepatitis C virus replication. PLoS Pathog. 2012;8: e1003056.
683 doi:10.1371/journal.ppat.1003056

684 29. Lumangtad LA, Bell TW. The signal peptide as a new target for drug design.
685 Bioorganic & Medicinal Chemistry Letters. 2020;30: 127115–8.
686 doi:10.1016/j.bmcl.2020.127115

687 30. Heijne G von. Membrane-protein topology. Nat. Rev. Mol. Cell Biol. 2006;7: 909–
688 918. doi:10.1038/nrm2063

689 31. Nilsson J, Persson B, Heijne G von. Comparative analysis of amino acid
690 distributions in integral membrane proteins from 107 genomes. Proteins. 2005;60:
691 606–616. doi:10.1002/prot.20583

692 32. Heijne G von. Control of topology and mode of assembly of a polytopic
693 membrane protein by positively charged residues. Nature. 1989;341.
694 doi:10.1038/341456a0

695 33. Izaguirre G. The Proteolytic Regulation of Virus Cell Entry by Furin and Other
696 Proprotein Convertases. Viruses. 2019;11: 837–19. doi:10.3390/v11090837

697 34. Lin S, Yang Y, Nan Y, Ma Z, Yang L, Zhang Y-J. The Capsid Protein of Hepatitis
698 E Virus Inhibits Interferon Induction via Its N-terminal Arginine-Rich Motif. Viruses.
699 2019;11: 1050–17. doi:10.3390/v11111050

700 35. Graff J, Torian U, Nguyen H, Emerson SU. A Bicistronic Subgenomic mRNA
701 Encodes both the ORF2 and ORF3 Proteins of Hepatitis E Virus. J Virol. 2006;80:
702 5919–5926. doi:10.1128/jvi.00046-06

703 36. Nair VP, Anang S, Subramani C, Madhvi A, Bakshi K, Srivastava A, et al.
704 Endoplasmic Reticulum Stress Induced Synthesis of a Novel Viral Factor Mediates
705 Efficient Replication of Genotype-1 Hepatitis E Virus. Meng X-J, editor. PLoS Pathog.
706 2016;12: e1005521. doi:10.1371/journal.ppat.1005521.s009

707 37. Blight KJ, Mckeating JA, Rice CM. Highly Permissive Cell Lines for Subgenomic
708 and Genomic Hepatitis C Virus RNA Replication. J Virol. 2002;76: 13001–13014.
709 doi:10.1128/jvi.76.24.13001-13014.2002

710 38. Graff J, Nguyen H, Yu C, Elkins WR, Claire MS, Purcell RH, et al. The Open
711 Reading Frame 3 Gene of Hepatitis E Virus Contains a cis-Reactive Element and
712 Encodes a Protein Required for Infection of Macaques. J Virol. 2005;79: 6680–6689.
713 doi:10.1128/jvi.79.11.6680-6689.2005

714 39. Cocquerel L, Wychowski C, Minner F, Penin F, Dubuisson J. Charged Residues
715 in the Transmembrane Domains of Hepatitis C Virus Glycoproteins Play a Major Role
716 in the Processing, Subcellular Localization, and Assembly of These Envelope
717 Proteins. J Virol. 2000;74: 3623–3633. doi:10.1128/jvi.74.8.3623-3633.2000

718 40. Orpana AK, Ho TH, Stenman J. Multiple Heat Pulses during PCR Extension
719 Enabling Amplification of GC-Rich Sequences and Reducing Amplification Bias. Anal
720 Chem. 2012;84: 2081–2087. doi:10.1021/ac300040j

721 41. McCloy RA, Rogers S, Caldon CE, Lorca T, Castro A, Burgess A. Partial
722 inhibition of Cdk1 in G 2phase overrides the SAC and decouples mitotic events. Cell
723 Cycle. 2014;13: 1400–1412. doi:10.4161/cc.28401

724 42. Marsollier L, Brodin P, Jackson M, Korduláková J, Tafelmeyer P, Carbonnelle E,
725 et al. Impact of Mycobacterium ulcerans Biofilm on Transmissibility to Ecological
726 Niches and Buruli Ulcer Pathogenesis. PLoS Pathog. 2007;3: e62-13.
727 doi:10.1371/journal.ppat.0030062

728

729

730 # Supporting information

731 ## Supporting figures

732

733 **S1 Fig. Colocalization analysis of ORF2 with the Golgi marker 130 (GM130) in**
734 **PLC3/HEV-p6 cells expressing ORF2wt or ARM/SP mutants.**

735

736 **S2 Fig. Colocalization analysis of ORF2 with the Importin-α1 in PLC3/HEV-p6**
737 **cells expressing ORF2wt and ARM/SP mutants.**

738

739 **S3 Fig. Transcriptomic analysis.**

740

741 **S4 Fig. Colocalization analysis of ORF2 with the exportin CRM1 in PLC3/HEV-**
742 **p6 cells expressing ORF2wt or NES mutants.**

743

744 **S5 Fig. Addressing of C2 constructs.**

745

746 **S6 Fig. Dose-response curves of PLC3 cells treated with the different drugs**
747 **used in this study.**

748

749 ## Supporting Materials and Methods

750

751 **RNA extraction and quantification.**
752 **Transcriptomic analysis.**

753

754 ## Supporting tables

755

756 **S1 Table: Primers of use to generate ORF2/CD4 chimeras/mutants.**

757 **S2 Table: Primers used for RT-qPCR of cellular genes.**

758

759 # Figure legends

760

761 **Fig 1. Kinetics of the subcellular localization of ORF2 protein in PLC3/HEV-p6**
762 **cells.** PLC3 cells were electroporated with HEV-p6 RNA and fixed at the indicated
763 timepoints p.e. Indirect immunofluorescence analysis was performed using the 1E6
764 anti-ORF2 antibody. Cells were analyzed by confocal microscopy (magnification x40).
765 Scale bar, 20 μm. Nuclear fluorescence intensity quantification was done using ImageJ
766 software (mean ± S.D., $n \geq 30$ cells, Friedman with Nemenyi test). ****$p < 0.0001$. Mock
767 electroporated PLC3 cells were used as controls.

768

769 **Fig 2. ORF2 contains an Arginine-Rich Motif (ARM) that is important for its**
770 **nuclear localization and host gene expression regulation.** (A) Schematic
771 sequence alignment of ORF2wt and ARM/SP mutants. (B) Subcellular localization of
772 ORF2wt and ARM/SP mutants. PLC3 cells were electroporated with wt and mutant
773 HEV-p6 RNAs. At 18 h.p.e, cells were processed for indirect immunofluorescence
774 using the 1E6 anti-ORF2 antibody (Ab) and analyzed by confocal microscopy
775 (magnification x63). Red = ORF2; Blue = DAPI. Scale bar, 20μm. Nuclear fluorescence
776 intensity quantification was done using ImageJ software (mean ± S.D., $n \geq 30$ cells,
777 Kruskal-Wallis with Conover's test). *$p < 0.05$, ****$p < 0.0001$. (C) Subcellular
778 fractionation of PLC3/HEV-p6 expressing ORF2wt and ARM/SP mutants at 10 d.p.e.
779 Fractionation was done using a subcellular protein fractionation kit for cultured cells.
780 ORF2 proteins were detected by WB with 1E6 Ab. Glycosylated ORF2 (ORF2g),
781 cleaved ORF2 (ORF2c), intracellular ORF2 (ORF2intra), nuclear ORF2intra (ORF2ni),
782 nuclear and cleaved ORF2intra (ORF2nc) are indicated. ORF3 protein in cell lysates
783 was detected with a rabbit anti-ORF3 Ab. Tubulin, ER marker Calnexin (CNX) and the

784 transcription factor SP1 used as a nuclear marker, were also detected to check the
785 quality of fractionation. Molecular mass markers are indicated on the right (kDa). (D)
786 Infectious titer determination and HEV RNA quantification in PLC3/HEV-p6 expressing
787 ORF2wt or mutant proteins. Extra- and intracellular viral particles were extracted at 10
788 d.p.e and used to infect naïve Huh7.5 cells for 3 days. Cells were next processed for
789 indirect immunofluorescence. ORF2-positive cells were counted and each positive cell
790 focus was considered as one FFU. Results were expressed in FFU/ml (n=4). Extra-
791 and intracellular viral RNAs were quantified at 10 d.p.e by RT-qPCR ($n \geq 5$) (mean ±
792 S.D., Kruskal-Wallis with Conover's test). *$p < 0.05$, **$p < 0.01$, ****$p < 0.0001$. (E)
793 Transcriptomic analysis of PLC3 cells expressing HEV-p6 wt, mutants or mock cells
794 performed with microarrays (Agilent SurePrint). Left - Heatmap of gene expression in
795 PLC3 cells expressing HEV-p6 wt, mutants or mock cells at 18 h.p.e. Color-code
796 represents the log fold-change (logFC) of gene expression in the indicated
797 comparisons. Right – STRING representation of the gene network specifically
798 modulated by ORF2. Bottom – Signaling pathways preferentially induced by the
799 nuclear translocation of ORF2 at 18 h.p.e. Transcriptomic results stem from 4
800 independent electroporation experiments.
801
802 **Fig 3. Nuclear export of the ORF2 protein.** (A) Analysis of ORF2 nuclear export in
803 inhibitors treated-PLC3/HEV-p6 cells. Cells were treated at 32 h.p.e with 20nM of
804 Leptomycin B (LepB), 100nM of Verdinexor (Verd) or diluent (EtOH or DMSO,
805 respectively) for 16h. Cells were processed for indirect immunofluorescence with the
806 1E6 anti-ORF2 Ab and analyzed by confocal microscopy (magnification x63). Red =
807 ORF2; Blue = DAPI. (B) Schematic representation of HEV-p6 ORF2 protein sequence
808 highlighting the three studied NES motifs (*i.e.,* NES9, NES10 and NES12). (C)

809 Subcellular localization of ORF2 NES mutants at 48 h.p.e. Red = ORF2; Blue = DAPI.
810 In A and C, the scale bars correspond to 20μm, and nuclear/cytosolic fluorescence
811 intensity quantification was done using ImageJ software (mean ± S.D., $n \geq 30$ cells,
812 Kruskal-Wallis with Conover's test). *$p < 0.05$, ***$p < 0.001$, ****$p < 0.0001$. (D)
813 Subcellular fractionation of PLC3/HEV-p6 expressing ORF2wt and NES mutants at 4
814 d.p.e. Fractionation was done using a subcellular protein fractionation kit for cultured
815 cells. ORF2 proteins were detected by WB with 1E6 Ab. Glycosylated ORF2 (ORF2g),
816 cleaved ORF2 (ORF2c), intracellular ORF2 (ORF2intra), nuclear ORF2intra (ORF2ni),
817 nuclear and cleaved ORF2intra (ORF2nc) are indicated. ORF3 protein in cell lysates
818 was detected with a rabbit anti-ORF3 Ab. Tubulin, ER marker Calnexin (CNX) and the
819 transcription factor SP1 used as a nuclear marker, were also detected to check the
820 quality of fractionation. Molecular mass markers are indicated on the right (kDa). (E)
821 Infectious titer determination in PLC3/HEV-p6 expressing ORF2wt or NES mutants.
822 Extra- and intracellular viral particles were extracted at 10 d.p.e and used to infect
823 naïve Huh7.5 cells for 3 days. Cells were next processed for indirect
824 immunofluorescence. ORF2-positive cells were counted and each positive cell focus
825 was considered as one FFU. Results were expressed in FFU/ml. (F) HEV RNA
826 quantification in PLC3/HEV-p6 expressing ORF2wt or NES mutants. Extra- and
827 intracellular viral RNAs were quantified at 10 d.p.e by RT-qPCR. In E and F, n=6, mean
828 ± S.D., Kruskal-Wallis with Conover's test, ***$p < 0.001$, ****$p < 0.0001$.
829
830 **Fig 4. Translocation and maturation of the glycosylated ORF2 forms.** (A) Dose-
831 response inhibition of ORF2g/c secretion in mycolactone-treated cells. PLC3/HEV-p6
832 and mock cells were treated for 24h with the indicated concentrations of mycolactone
833 (in nM) or maximal volume of the vehicle, ethanol (indicated as 0 nM). Supernatants

834 (SN) and lysates (Cells) were collected and ORF2 proteins were detected by WB using
835 the 1E6 Ab. Tubulin served as control protein loading. (B) Schematic representation of
836 ORF2i/g/c proteins and recognition sites of P1H1 and P3H2 antibodies used to
837 discriminate the different ORF2 forms. SP, signal peptide. PC, proprotein convertase.
838 Glycans are in black. (C) Immunoprecipitation of ORF2 proteins in SN and lysates of
839 PLC3/HEV-p6 cells by P1H1, P3H2 and isotype control (CTL) antibodies immobilized
840 on magnetic beads. ORF2 proteins were detected by WB using the 1E6 Ab. (D-F)
841 PLC3/HEV-p6 cells were treated for 72h with the indicated concentrations of CMK,
842 D6R or SSM3 (in μM) or DMSO diluent (indicated as 0 μM). Supernatants (SN) and
843 lysates (Cells) were collected. SN were immunoprecipitated with P1H1 and P3H2
844 antibodies and ORF2 proteins were detected by WB using the 1E6 Ab. ORF2intra, αV-
845 Integrin (IntαV) and Tubulin (Tub) were detected in cell lysates. αV-pro-integrin
846 (ProintαV) corresponds to the non-maturated αV-integrin. ORF2g* corresponds to the
847 ORF2g immunoprecipitated by the P1H1 Ab. Molecular mass markers are indicated
848 on the right (kDa).
849
850 **Fig 5. The ORF2 ARM is the regulator of ORF2 addressing.** Schematic
851 representation of ORF2wt and CD4wt proteins. ORF2 sequences are in blue. ARM
852 residues are highlighted in red. CD4 sequences are in green. (A) H7-T7-IZ cells were
853 transfected with pTM plasmids expressing wt, mutant or chimeric ORF2 proteins.
854 Twenty-four hours post-transfection, cells were fixed and processed for ORF2 staining
855 (in red). Nuclei are in blue. Representative confocal images are shown together with
856 ORF2/DAPI merge images (magnification x63). Blue dots observed in some pictures
857 are DAPI-stained transfected plasmids. A schematic representation of each construct
858 is shown on the left. Scale bar, 20μm. (B) Nuclear-to-cytoplasmic ORF2 staining ratio

859 in H7-T7-IZ cells expressing mutant and chimeric ORF2 proteins. Quantification was
860 done using ImageJ software (mean ± S.D., $n \geq 30$ cells, Kruskal-Wallis with Conover's
861 test). **$p < 0.01$, ****$p < 0.0001$. (C) Subcellular fractionation of H7-T7-IZ cells
862 expressing mutant and chimeric ORF2 proteins at 24h post-transfection. Fractionation
863 was done using a subcellular protein fractionation kit for cultured cells. ORF2 proteins
864 were detected by WB with 1E6 Ab. Tubulin, Calnexin (CNX) and Lamin B1 were also
865 detected to control the quality of fractionation. Molecular mass markers are indicated
866 on the right (kDa).
867
868 **Fig 6. CD4 addressing by the ORF2 ARM.** Schematic representation of ORF2wt and
869 CD4wt proteins. SP ORF2 residues are shown in blue. ARM residues are highlighted
870 in red. CD4 sequences are in green. (A) and (C), H7-T7-IZ cells were transfected with
871 pTM plasmids expressing CD4wt or chimeric C4 and C5 proteins. Twenty-four hours
872 post-transfection, cells were fixed and processed for CD4 staining (in green). Nuclei
873 are in blue. Representative confocal images are shown together with CD4/DAPI merge
874 images. Blue dots observed in some pictures are DAPI-stained transfected plasmids.
875 A schematic representation of each construct is shown on the left. Scale bar, 20μm.
876 (B) Nuclear-to-cytoplasmic CD4 staining ratio in H7-T7-IZ cells expressing CD4wt or
877 chimeric proteins. Quantification was done using ImageJ software (mean ± S.D., $n \geq$
878 30 cells, Kruskal-Wallis with Conover's test). ****$p < 0.0001$. (D) Subcellular
879 fractionation of H7-T7-IZ cells expressing CD4wt or chimeric proteins at 24h post-
880 transfection. Fractionation was done using the subcellular protein fractionation kit for
881 cultured cells. CD4 proteins were detected by WB with a rabbit polyclonal anti-CD4
882 Ab. Tubulin, Calnexin (CNX) and Lamin B1 were also detected to control the quality of
883 fractionation. Molecular mass markers are indicated on the right (kDa).

884

885 **Fig 7. The ORF2 ARM regulates the topology of ORF2 SP.** A schematic
886 representation of differential permeabilization process with Triton X-100 and Digitonin
887 is shown. Representative images of the differential detection of two epitopes on the
888 ER-membrane associated Calnexin (CNX) used to assess the permeabilization
889 conditions are shown. H7-T7-IZ cells were transfected with pTM plasmids expressing
890 wt, mutant or chimeric ORF2 proteins. Twenty-four hours post-transfection, cells were
891 fixed, permeabilized with either Triton X-100 or Digitonin, and processed for ORF2
892 staining (in red). Nuclei are in blue. Representative confocal merge ORF2/DAPI
893 images are shown (magnification x63). Blue dots observed in some pictures are DAPI-
894 stained transfected plasmids. A schematic representation of each construct is shown
895 on the left and its predicted topology on the right. Blue and red asterisks correspond
896 to 5R/5A and PSG/3R mutations, respectively. Scale bar, 20μm.

897

898 **Fig 8. The ORF2 ARM is also able to control the topology of CD4 SP.** A schematic
899 representation of differential permeabilization process with Triton X-100 and Digitonin
900 is shown. Representative images of the differential detection of two epitopes on the
901 ER-membrane associated Calnexin (CNX) in the used permeabilization conditions are
902 shown. H7-T7-IZ cells were transfected with pTM plasmids expressing CD4wt or
903 chimeric C4 and C5 proteins. Twenty-four hours post-transfection, cells were fixed,
904 permeabilized with either Triton X-100 or Digitonin, and processed for CD4 staining (in
905 green). Nuclei are in blue. Representative confocal CD4/DAPI merge images are
906 shown. Blue dots observed in some pictures are DAPI-stained transfected plasmids.
907 A schematic representation of each construct is shown on the left and its predicted

908 topology on the right. Blue and red asterisks correspond to 5R/5A and PSG/3R
909 mutations, respectively. Scale bar, 20μm.
910
911 **Fig 9. Model of ORF2 addressing regulation by ARM.** (A) The signal recognition
912 particle (SRP) recognizes the hydrophobic signal peptide (SP) of the ORF2 nascent
913 chain as it emerges from a translating ribosome. The ribosome-nascent chain-SRP
914 complex is targeted to the membrane and interacts with the SRP receptor, resulting in
915 the release of the SP and docking of the ribosome–nascent chain complex to the
916 Sec61 translocon. The ORF2 SP initially inserts head-on in an N_{exo}/C_{cyt} orientation,
917 then inverts its orientation to N_{cyt}/C_{exo}. (B) The C-terminal end of SP is exposed to ER
918 lumen and is cleaved by signal peptidase, generating a new N-terminus. Translation
919 then resumes, and the nascent ORF2 protein is translocated into the ER lumen where
920 it is glycosylated and likely undergoes maturation by a proprotein convertase. This
921 pathway generates the ORF2g/c forms. (C) For a fraction of ORF2 nascent polypeptide
922 chains, the ARM leads the ORF2 SP to retain its N_{exo}/C_{cyt} orientation and integrates as
923 reverse signal-anchor, according to the positive-inside rule. The ORF2 protein
924 anchored to the cytosolic side of membrane is likely processed by an intramembrane
925 protease to generate the ORF2i/ORF2 intra protein that is translocated into the nucleus
926 and assembles into viral particles.

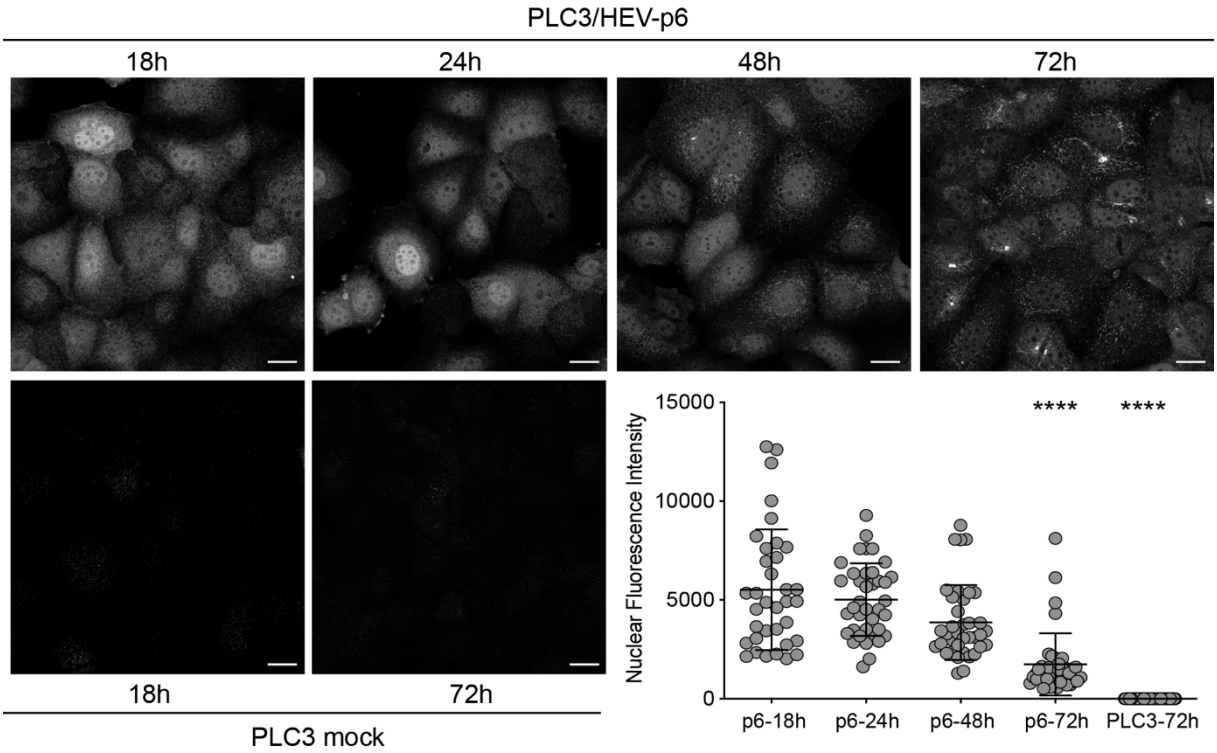
PLC3/HEV-p6
18h
24h
48h
72h
18h
72h
PLC3 mock
Nuclear Fluorescence Intensity
15000
10000
5000
0
****
****
p6-18h
p6-24h
p6-48h
p6-72h
PLC3-72h

Fig. 1

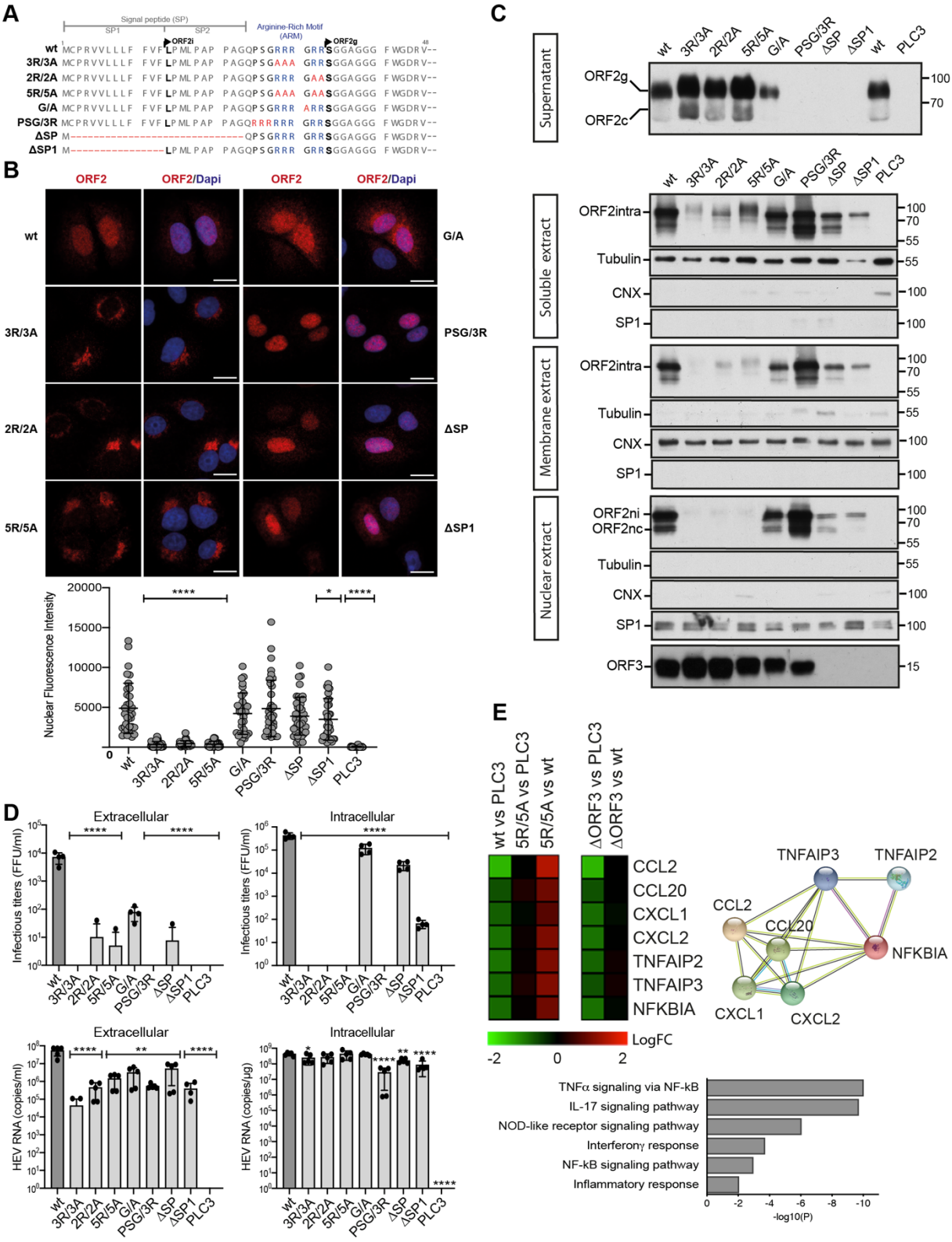
A
Signal peptide (SP)
SP1
SP2
Arginine-Rich Motif (ARM)
ORF2i
ORF2g
wt
3R/3A
2R/2A
5R/5A
G/A
PSG/3R
ΔSP
ΔSP1
B
ORF2
ORF2/Dapi
Nuclear Fluorescence Intensity
C
Supernatant
Soluble extract
Membrane extract
Nuclear extract
ORF2g
ORF2c
ORF2intra
Tubulin
CNX
SP1
ORF2ni
ORF2nc
ORF3
PLC3
D
Extracellular
Intracellular
Infectious titers (FFU/ml)
HEV RNA (copies/ml)
HEV RNA (copies/µg)
E
wt vs PLC3
5R/5A vs PLC3
5R/5A vs wt
ΔORF3 vs PLC3
ΔORF3 vs wt
CCL2
CCL20
CXCL1
CXCL2
TNFAIP2
TNFAIP3
NFKBIA
LogFC
TNFα signaling via NF-kB
IL-17 signaling pathway
NOD-like receptor signaling pathway
Interferonγ response
NF-kB signaling pathway
Inflammatory response
-log10(P)

Fig. 2

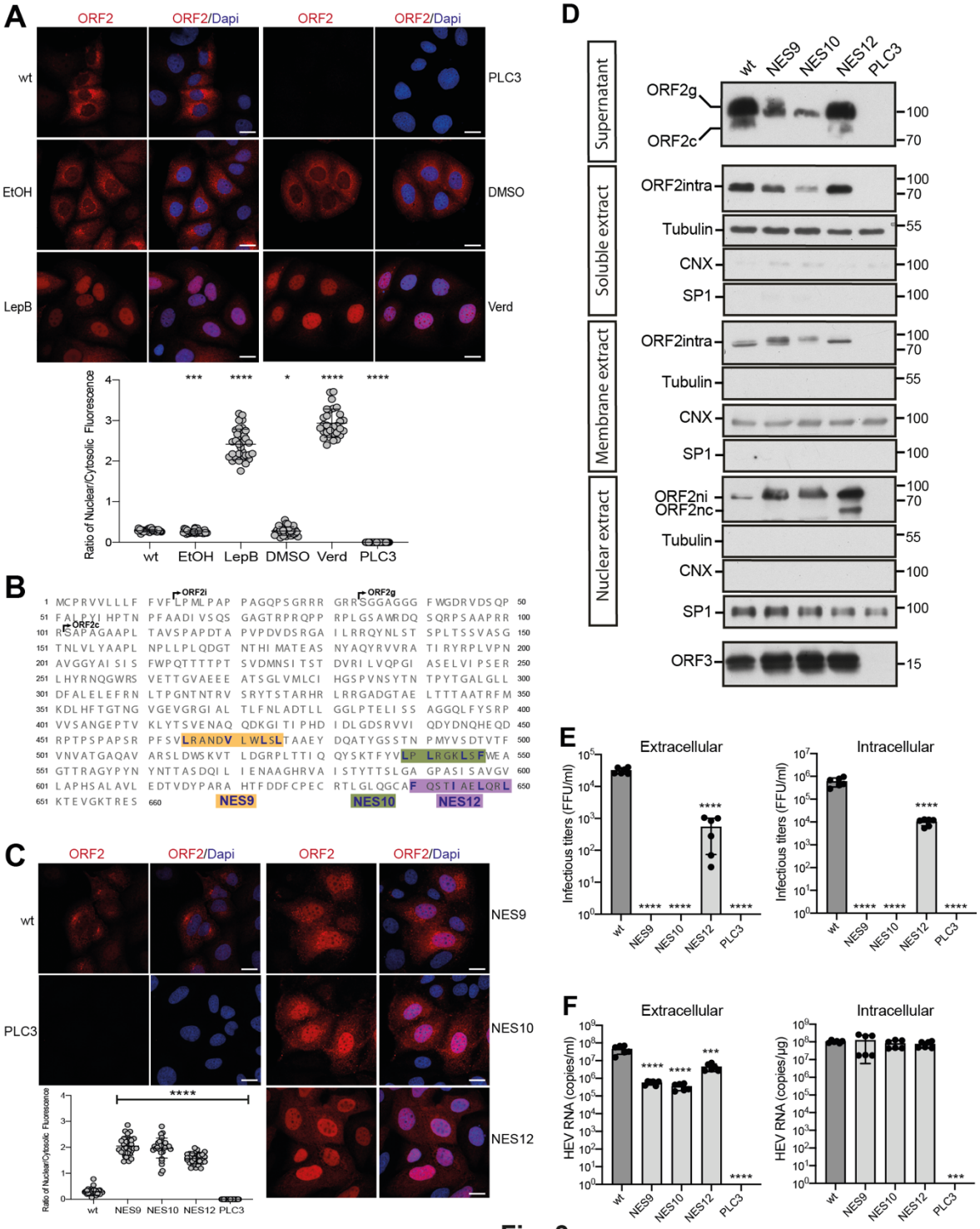
A
ORF2
ORF2/Dapi
ORF2
ORF2/Dapi
wt
PLC3
EtOH
DMSO
LepB
Verd
Ratio of Nuclear/Cytosolic Fluorescence
wt
EtOH
LepB
DMSO
Verd
PLC3
B
ORF2i
ORF2g
ORF2c
NES9
NES10
NES12
C
ORF2
ORF2/Dapi
ORF2
ORF2/Dapi
wt
PLC3
NES9
NES10
NES12
Ratio of Nuclear/Cytosolic Fluorescence
wt
NES9
NES10
NES12
PLC3
D
Supernatant
Soluble extract
Membrane extract
Nuclear extract
wt
NES9
NES10
NES12
PLC3
ORF2g
ORF2c
ORF2intra
Tubulin
CNX
SP1
ORF2ni
ORF2nc
ORF3
E
Extracellular
Intracellular
Infectious titers (FFU/ml)
wt
NES9
NES10
NES12
PLC3
F
Extracellular
Intracellular
HEV RNA (copies/ml)
HEV RNA (copies/µg)
wt
NES9
NES10
NES12
PLC3

Fig. 3

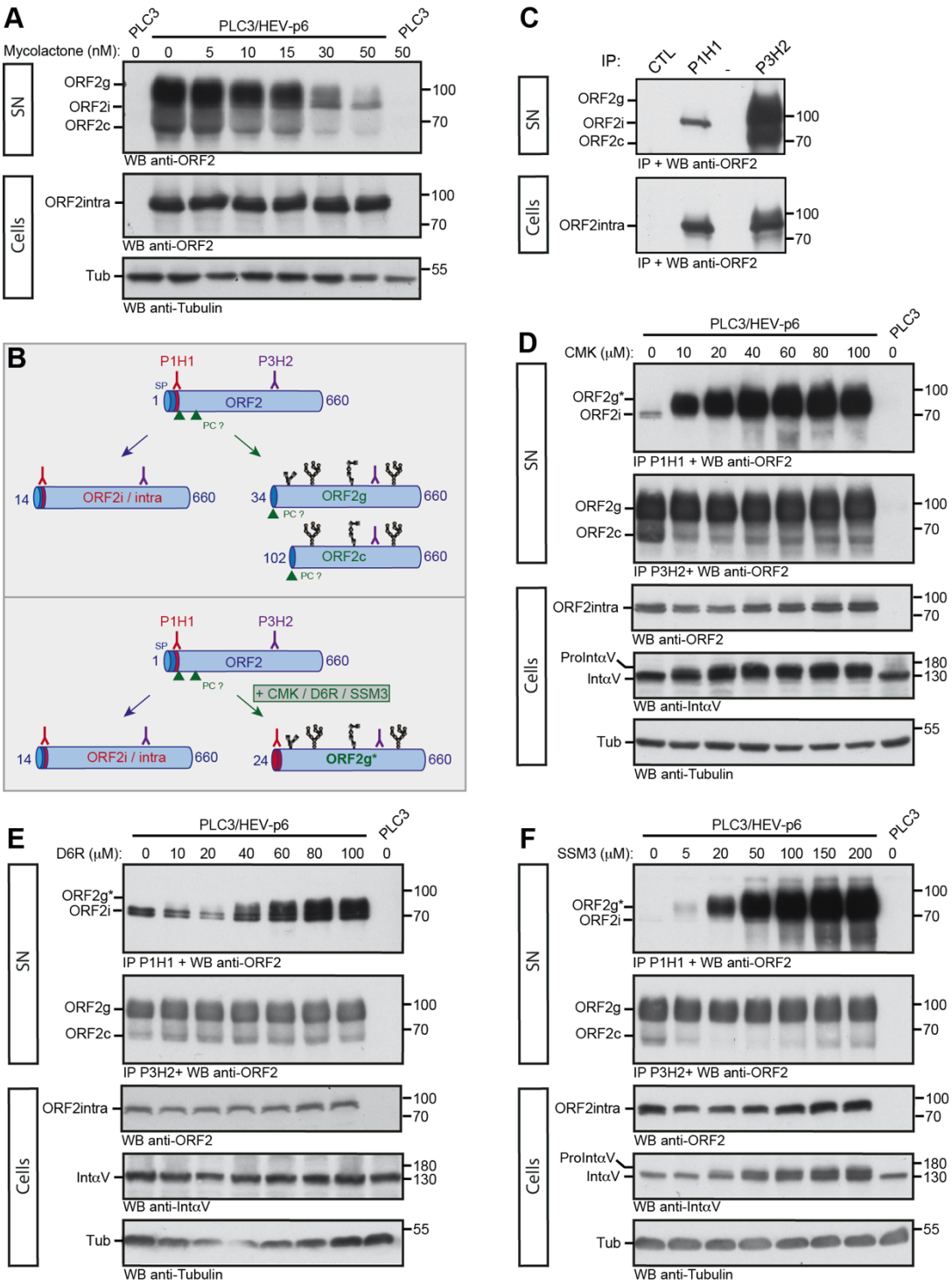
A
PLC3
PLC3/HEV-p6
PLC3
Mycolactone (nM): 0 0 5 10 15 30 50 50
SN
ORF2g
ORF2i
ORF2c
100
70
WB anti-ORF2
Cells
ORF2intra
100
70
WB anti-ORF2
Tub
55
WB anti-Tubulin
B
P1H1
P3H2
SP
1
ORF2
660
PC ?
14
ORF2i / intra
660
34
ORF2g
660
PC ?
102
ORF2c
660
PC ?
P1H1
P3H2
SP
1
ORF2
660
PC ?
+ CMK / D6R / SSM3
14
ORF2i / intra
660
24
ORF2g*
660
C
IP:
CTL
P1H1
-
P3H2
SN
ORF2g
ORF2i
ORF2c
100
70
IP + WB anti-ORF2
Cells
ORF2intra
100
70
IP + WB anti-ORF2
D
PLC3/HEV-p6
PLC3
CMK (μM): 0 10 20 40 60 80 100 0
SN
ORF2g*
ORF2i
100
70
IP P1H1 + WB anti-ORF2
ORF2g
ORF2c
100
70
IP P3H2+ WB anti-ORF2
Cells
ORF2intra
100
70
WB anti-ORF2
ProIntαV
IntαV
180
130
WB anti-IntαV
Tub
55
WB anti-Tubulin
E
PLC3/HEV-p6
PLC3
D6R (μM): 0 10 20 40 60 80 100 0
SN
ORF2g*
ORF2i
100
70
IP P1H1 + WB anti-ORF2
ORF2g
ORF2c
100
70
IP P3H2+ WB anti-ORF2
Cells
ORF2intra
100
70
WB anti-ORF2
IntαV
180
130
WB anti-IntαV
Tub
55
WB anti-Tubulin
F
PLC3/HEV-p6
PLC3
SSM3 (μM): 0 5 20 50 100 150 200 0
SN
ORF2g*
ORF2i
100
70
IP P1H1 + WB anti-ORF2
ORF2g
ORF2c
100
70
IP P3H2+ WB anti-ORF2
Cells
ORF2intra
100
70
WB anti-ORF2
ProIntαV
IntαV
180
130
WB anti-IntαV
Tub
55
WB anti-Tubulin

Fig. 4

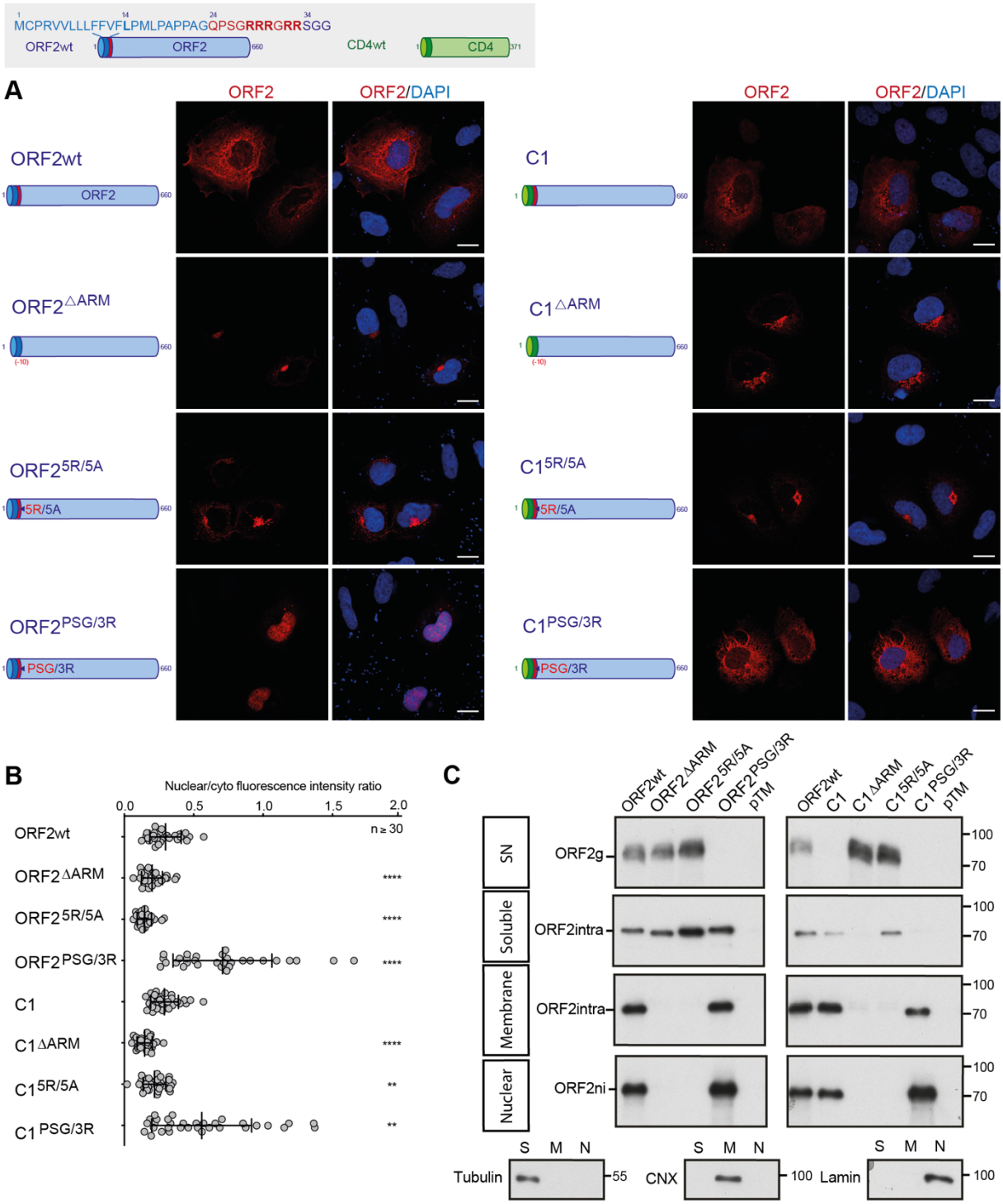
MCPRVVLLLFFVFLPMLPAPPAGQPSGRRRGRRSGG
ORF2wt
ORF2
CD4wt
CD4
A
ORF2
ORF2/DAPI
ORF2wt
C1
ORF2△ARM
C1△ARM
ORF2 5R/5A
C1 5R/5A
ORF2 PSG/3R
C1 PSG/3R
B
Nuclear/cyto fluorescence intensity ratio
0.0
0.5
1.0
1.5
2.0
n ≥ 30
ORF2wt
ORF2△ARM
ORF2 5R/5A
ORF2 PSG/3R
C1
C1△ARM
C1 5R/5A
C1 PSG/3R
****
**
C
ORF2wt
ORF2△ARM
ORF2 5R/5A
ORF2 PSG/3R
pTM
C1
C1△ARM
C1 5R/5A
C1 PSG/3R
SN
Soluble
Membrane
Nuclear
ORF2g
ORF2intra
ORF2ni
100
70
S M N
Tubulin
55
CNX
Lamin

Fig. 5

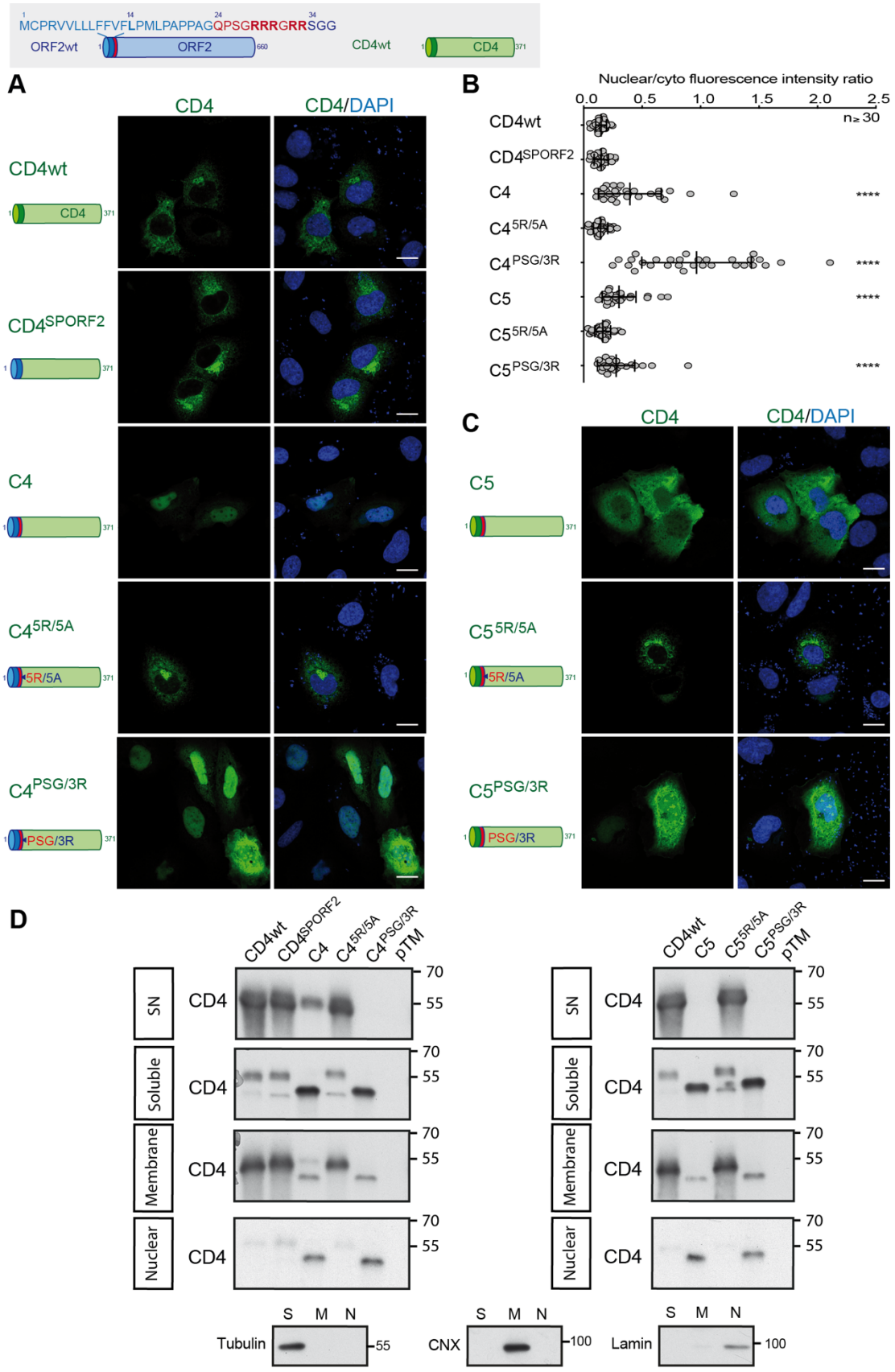
MCPRVVLLLFFVFLPMLPAPPAGQPSGRRRGRRSGG
ORF2wt
ORF2
CD4wt
CD4
A
CD4
CD4/DAPI
CD4wt
CD4SPORF2
C4
C4 5R/5A
C4 PSG/3R
5R/5A
PSG/3R
B
Nuclear/cyto fluorescence intensity ratio
n≥ 30
CD4wt
CD4SPORF2
C4
C4 5R/5A
C4 PSG/3R
C5
C5 5R/5A
C5 PSG/3R
****
C
C5
C5 5R/5A
C5 PSG/3R
D
CD4wt
CD4SPORF2
C4
C4 5R/5A
C4 PSG/3R
pTM
C5
C5 5R/5A
C5 PSG/3R
SN
Soluble
Membrane
Nuclear
CD4
Tubulin
CNX
Lamin
S M N

Fig. 6

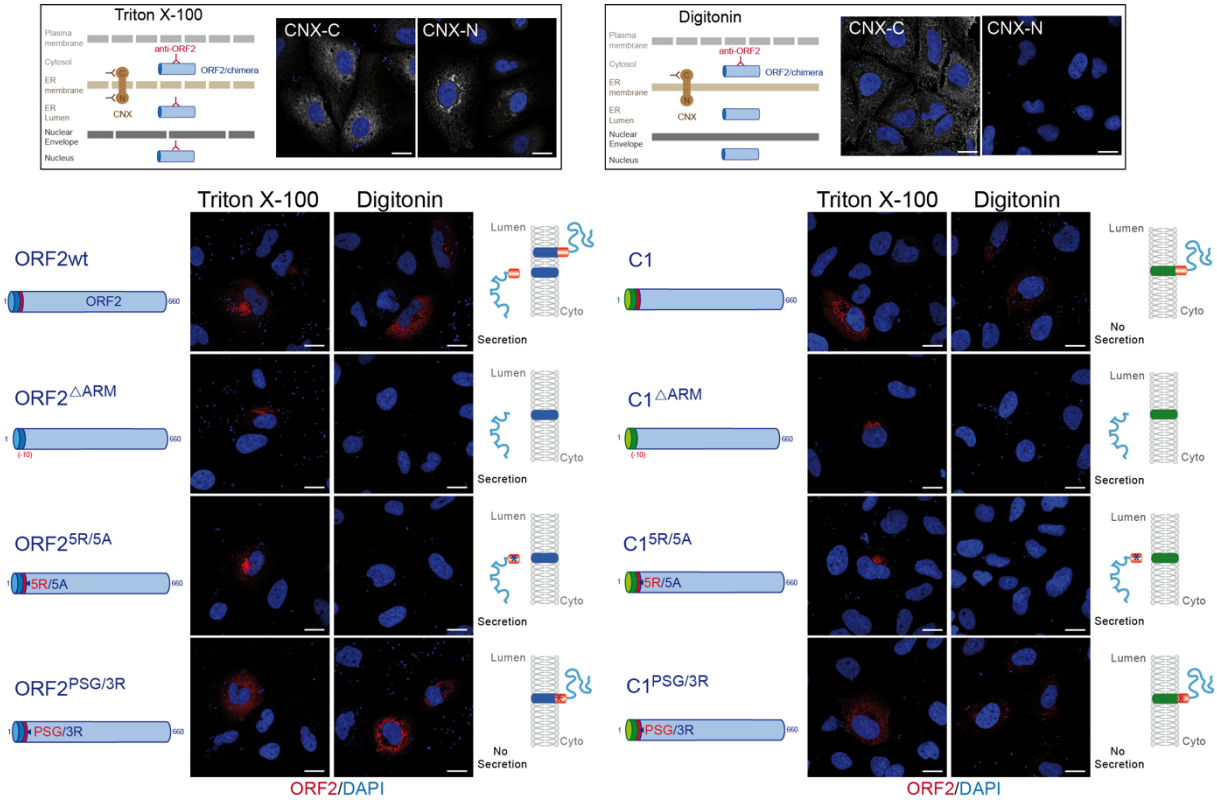
Triton X-100
Plasma membrane
Cytosol
ER membrane
ER Lumen
Nuclear Envelope
Nucleus
anti-ORF2
ORF2/chimera
CNX
CNX-C
CNX-N
Digitonin
Triton X-100
Digitonin
ORF2wt
ORF2
ORF2△ARM
ORF2^5R/5A
5R/5A
ORF2^PSG/3R
PSG/3R
Lumen
Cyto
Secretion
No Secretion
C1
C1△ARM
C1^5R/5A
C1^PSG/3R
ORF2/DAPI

Fig. 7

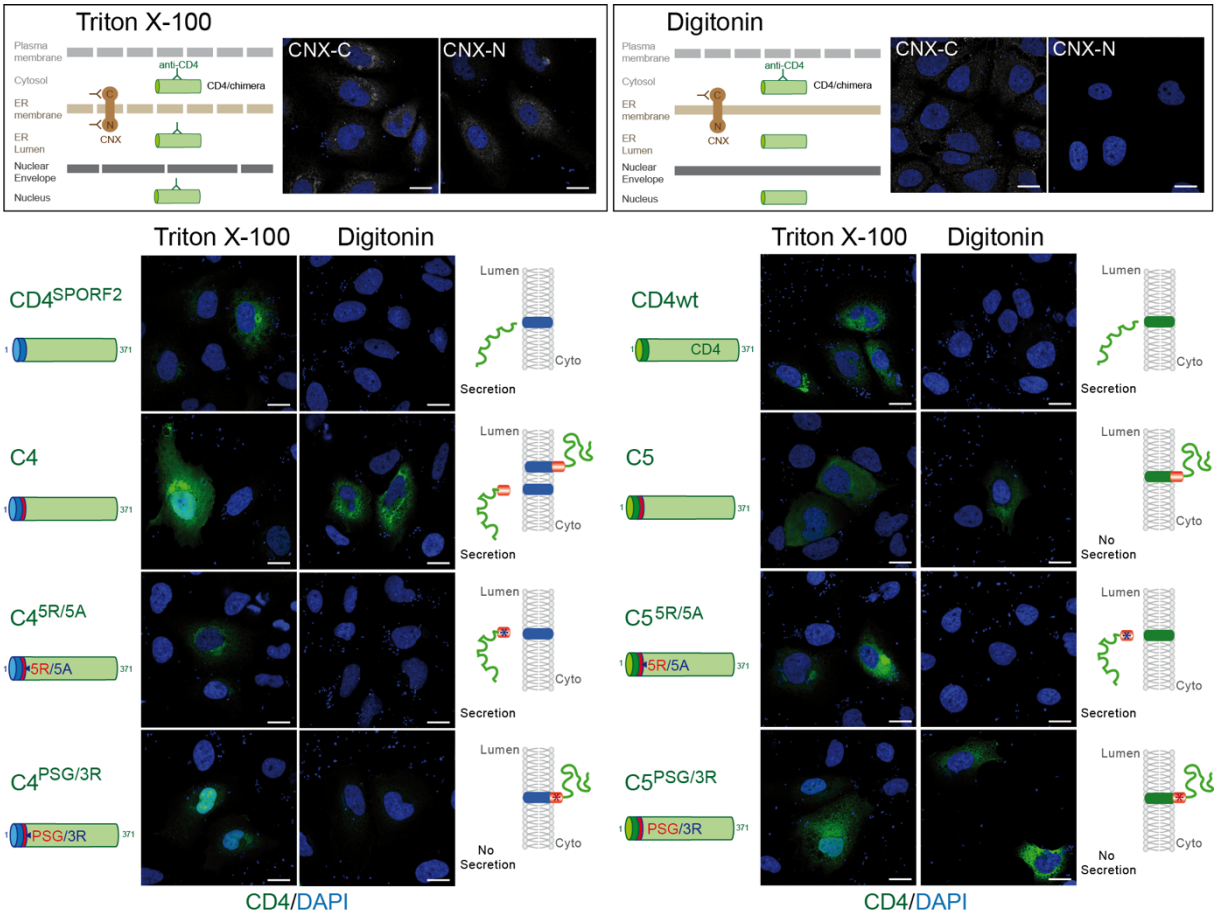
Triton X-100
Plasma membrane
Cytosol
ER membrane
ER Lumen
Nuclear Envelope
Nucleus
anti-CD4
CD4/chimera
CNX
CNX-C
CNX-N
Digitonin
Triton X-100
Digitonin
CD4SPORF2
C4
C45R/5A
C4PSG/3R
CD4wt
C5
C55R/5A
C5PSG/3R
5R/5A
PSG/3R
CD4
Lumen
Cyto
Secretion
No Secretion
CD4/DAPI

Fig. 8

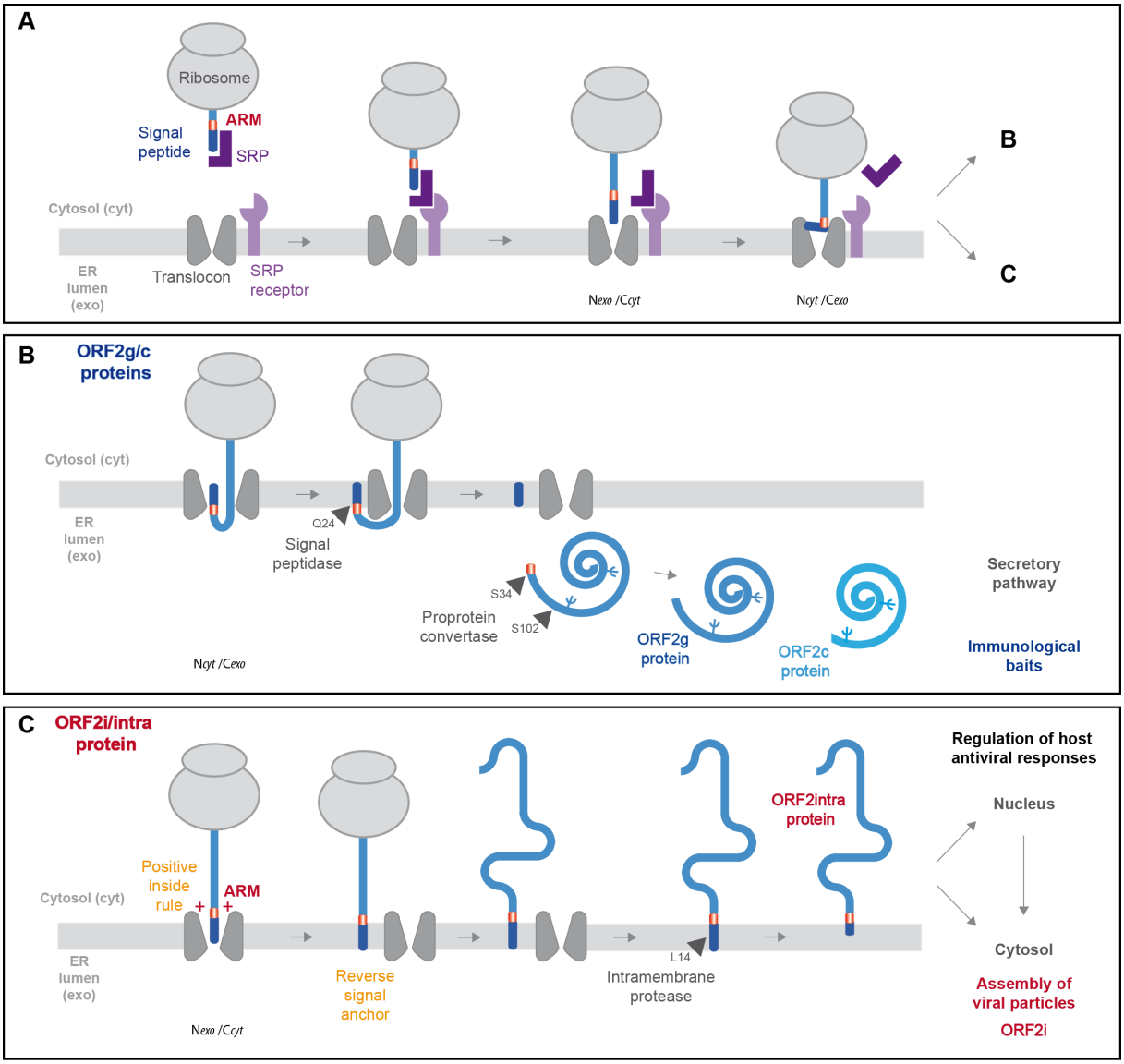
A
Ribosome
ARM
Signal peptide
SRP
Cytosol (cyt)
ER lumen (exo)
Translocon
SRP receptor
Nexo /Cyt
Nyt /Cexo
B
C
B
ORF2g/c proteins
Cytosol (cyt)
ER lumen (exo)
Q24
Signal peptidase
S34
S102
Proprotein convertase
ORF2g protein
ORF2c protein
Nyt /Cexo
Secretory pathway
Immunological baits
C
ORF2i/intra protein
Positive inside rule
ARM
Cytosol (cyt)
ER lumen (exo)
Reverse signal anchor
L14
Intramembrane protease
ORF2intra protein
Nexo /Cyt
Regulation of host antiviral responses
Nucleus
Cytosol
Assembly of viral particles
ORF2i

Fig. 9